

5/6/99

MICROMACHINED STIMULATING ELECTRODES

Final Report

Contract NIH-NINDS-N01-NS-5-2335



Submitted to the

Neural Prosthesis Program

National Institute of Neurological Disorders and Stroke
National Institutes of Health
Bethesda, MD 20892

by the

Center for Integrated MicroSystems

Department of Electrical Engineering and Computer Science
The University of Michigan
Ann Arbor, MI 48109-2122

March 1999

MICROMACHINED STIMULATING ELECTRODES

Summary

This contract has advanced the state-of-the-art in micromachined stimulating electrode arrays in a number of areas. Improvements in the design of the stimulating sites have eliminated the iridium adhesion problems seen in the past and ensured good step coverage of the site metal into the contact vias. Titanium nitride is being explored as a possible to activated iridium (IrO) as a site material with promising results, and both titanium silicide and tantalum have been shown capable of reducing the resistance of polysilicon interconnect lines by as much as an order of magnitude. A variety of passive probe designs have been fabricated for internal and external users, including a flexible 22-site stimulating probe which could serve as a prototype for an improved cochlear prosthesis. These devices have been conformally coated with parylene for mechanical strength; the sites are exposed using laser ablation followed by an oxygen plasma to remove residual polymer. The use of alternative etch-stop techniques for defining the probe substrate have also been explored, and the use of a bulk n+ buried sacrificial layer has been found capable of forming lightly-doped probe substrates in a single-sided process. This process would allow the formation of distributed circuitry on probe shanks; however, the overall process is somewhat more complex than the boron etch-stop now used. The boron process will be retained for penetrating probes, although for applications such as the cochlear probe the buried layer process should be explored further.

The process technology for active probes has been improved to the point where it now allows high yield on a repeatable basis. Improved circuit contacts are ensured using thick titanium plugs under the aluminum circuit metal, and hillocking is avoided in the pad areas using layered titanium-aluminum stacks. Attack of the circuit area during the final probe release etch is prevented using dielectric bridges at the convex corners of the circuit area, and early release of the probe shanks is aided using deep dry etching to allow shank undercutting from the front of the wafer.

A 64-site 4-channel stimulating probe (STIM-2B) with off-chip current generation has been developed under this contract. The probe accepts a serial bit stream to select four of the 64 sites using four 16:1 multiplexers. Any site can be set to either stimulation or recording, with on-chip band-limited preamplifiers provided for each channel. The probe allows impedance testing from off-chip as well as parallel activation of the various sites. The probes have been characterized in-vitro and found to provide performance very close to design targets. They are now being used in-vivo to map connections between the dorsal cochlear nucleus and the inferior colliculus in guinea pig. Mapping that would be impossible using individual wire electrodes can be performed automatically without physically moving the probes via electronic site positioning/selection. Versions of this probe that are compatible with use in three-dimensional arrays (STIM-3B) have also been realized along with the required platforms and spacers. Microassemblies as large as 1024 sites and 64 parallel channels can be realized and are being assembled.

The previously-designed high-end probe STIM-2 was fabricated and tested in-vitro under this contract. Most aspects of these probes performed close to expectations; however, some areas for design improvement were identified, including the need for redesigned digital-to-analog converters for stimulus current generation. We are now implementing the needed design changes. A modular DSP-based external user interface for both STIM-2B/3B and STIM-2/3 has been developed and is now in use with these probes. The interface includes a graphical user interface to make the probes simple to use.

MICROMACHINED STIMULATING ELECTRODES

Table of Contents

Summary
Table of Contents

1. Introduction	1
2. Passive Thin-Film Stimulating Electrode Arrays	2
2.1 Basic Probe Fabrication and Site Engineering	3
2.2 Three-Dimensional Microelectrode Arrays	10
2.3 A Sacrificial Bulk Micromachining Technology	12
3. Active Stimulating Arrays: Basic Design and Fabrication	17
4. STIM-2B/3B: A Multiplexed 4-Channel 64-Site Probe with Off-Chip Current Generation	21
5. STIM-2: A 64-Site 8-Channel Active Stimulating Probe with On-Chip Current Generation	32
6. An External Interface for Active Stimulating Microelectrode Arrays	47
7. Conclusions	51
8. References	52

MICROMACHINED STIMULATING ELECTRODES

1. Introduction

This final report is being written to summarize accomplishments on Contract NIH-NINDS-N01-NS-5-2335, which began in December 1995 and ended in February 1999. The contract continued our work to develop dense high-performance arrays of micromachined stimulating electrodes for use in the central nervous system. These arrays are intended to allow highly selective stimulation of neuronal systems in terms of stimulus amplitude, time, and spatial location. Thus, the arrays should permit many small clusters of neurons to be stimulated independently, both to allow improved studies of neural systems at the circuit level and, especially, as a basis for practical neural prostheses. The primary initial target here is intracortical microstimulation of the visual cortex as the basis for a visual prosthesis; however, the same techniques and many of the same structures should also be applicable to auditory, motor, and other prostheses. In addition, direct application of the technology to the suppression of epileptic seizures and the tremors associated with Parkinson's disease is also a possibility.

Our approach to the fabrication of the needed electrode arrays continues to be based on merging high-performance silicon micromachining technology with on-chip integrated circuits. Silicon, in thin ($<20\mu\text{m}$) microstructures, is an extremely strong and flexible material that can be etched with a precision far greater than that of any other known material. In addition, when silicon is used as the supporting substrate for the probes, circuitry can be embedded directly in it to allow the control of many sites from very few input leads. No bonds or externally-visible contacts need be used; in addition, the output leads themselves can be realized as multi-strand multi-lead ribbon cables, hermetically sealed using the same dielectric coatings used for the probes themselves. In fact, the leads can be fabricated as part of the probes, yielding a completely sealed structure in which the only bonds required are within the final percutaneous plug. This technology now permits chronic stimulation and single-unit recording for several weeks on a rather routine basis.

In developing such electrode arrays, the yield of the associated process is of critical importance as is its compatibility with eventual fabrication in a commercial foundry. Although the technology levels associated with these probes are high for a university fabrication facility, they are very conservative relative to the levels now used for industrial VLSI circuits. The micromachining steps permit yields above 90 percent, so that they are not a limiting factor in the overall process. The probe development work at Michigan has, in fact, been a technology driver for sensor development not only at Michigan but worldwide [Wise 91-1, Wise 96], both in terms of technology and in terms of circuit interfaces. Extensions of this work have fueled microstructures for the measurement of flow, pressure, acceleration, tactile and thermal images, and many other variables. Some of these efforts are already beginning to appear as commercial products, and we would hope that the probes will eventually emerge in this form as well. Also significant is the fact that with a single additional masking step, microchannels can be formed in the probe substrate to allow chemical drug delivery at the cellular level in combination with electrical recording and stimulation. This promises to allow significant new neuropharmacological studies and perhaps eventually therapeutic procedures that have been impossible in the past [Chen 97].

During this past contract, significant progress has been made in several areas. Low-resistance interconnect materials have been evaluated as an alternative to the polysilicon previously used. This is especially important for stimulating electrodes due to the larger current they carry as compared with recording electrode arrays. We have also evaluated alternative micromachining techniques compared with the boron etch-stop for substrate definition. While the use of an n+ buried layer allows probe definition using a bulk sacrificial etch from the front of the wafer and allows the formation of circuitry within the material, the overall process is more complex than the boron etch-stop. Thus, the existing process will be maintained for the present, at least for penetrating electrodes. For flexible cochlear electrodes, the bulk sacrificial n+ process remains attractive. We have improved our micromachining techniques to broaden the process window in forming on-chip circuitry using the boron etch-stop and are now realizing active stimulating probes with high yield. Our high-end 64-site 8-channel stimulating probe with on-chip current generation (STIM-2) has been redesigned and is ready for fabrication. In addition, we have fabricated and tested an intermediate probe, STIM-2B/3B during the past contract. This is a 64-site 4-channel probe in which each selected site can be used for recording or for stimulation. These probes are currently being used for exploring the organization of connections between the dorsal cochlear nucleus (DCN) and the inferior colliculus (IC) in guinea pig.

This report will describe work in each of the above areas. Recent publications by our group and by others using these probes are separately attached.

2. Passive Thin-Film Stimulating Electrode Arrays

The basic probe structure is shown in Fig. 1. A micromachined silicon substrate supports an array of thin-film conductors that are insulated above and below by deposited dielectrics of silicon dioxide and silicon nitride. Openings in the upper dielectrics define stimulating or recording sites along the probe shank, which are inlaid with iridium oxide for interfacing to the tissue. At the rear of the probe, circuitry provides a multiplexed interface to the output leads, which connect to a remote percutaneous plug.

In forming these probe structures, a diffused boron etch-stop is used for silicon substrate definition. This allows reproducible substrate formation, dimensional control to better than $1\mu\text{m}$, and a minimum shank width of $20\mu\text{m}$ or less [Najafi 90-1]. This is accomplished with a single-sided process using wafers of standard thickness. When reactive ion etching (RIE) is used to recess the field area of the chip (between the probes) from the front, shanks as narrow as $5\mu\text{m}$ can be produced. Probe size is limited not by technology but by the strength required to penetrate the pia arachnoid. We have shown that oxide/nitride stress-compensated dielectrics, in combination with interconnects of polysilicon, tantalum, or refractory silicides, are a suitable encapsulation for the probe shanks for at least one year and probably much longer [Hetke 94]. Site impedances (typically about $1\text{M}\Omega$ for recording sites) remain relatively stable for over one year in-vivo. We have also demonstrated the integration of high-performance CMOS circuitry in the probe substrates, both for recording and for stimulation [Ji 90, Tanghe 92, Lund 94, Kim 96, Bai 98]. The basic probe process has been also used to form multistrand multi-conductor silicon ribbon cables for use in connecting the probes to the outside world [Hetke 94]. These cables offer minimal tethering forces, can be built directly into the probe itself, and can be completely surrounded by a conducting shield, protecting the dielectrics from the extracellular fluid. The cables have been tested for over four years under bias in saline without significant degradation. Finally, we have formed single-chip multichannel rf

telemetry interfaces capable of supplying power and control data to implanted electrodes for use in muscle stimulation [Von Arx 97]. There are no off-chip components, and the antenna is electroplated directly over the circuitry on the chip.

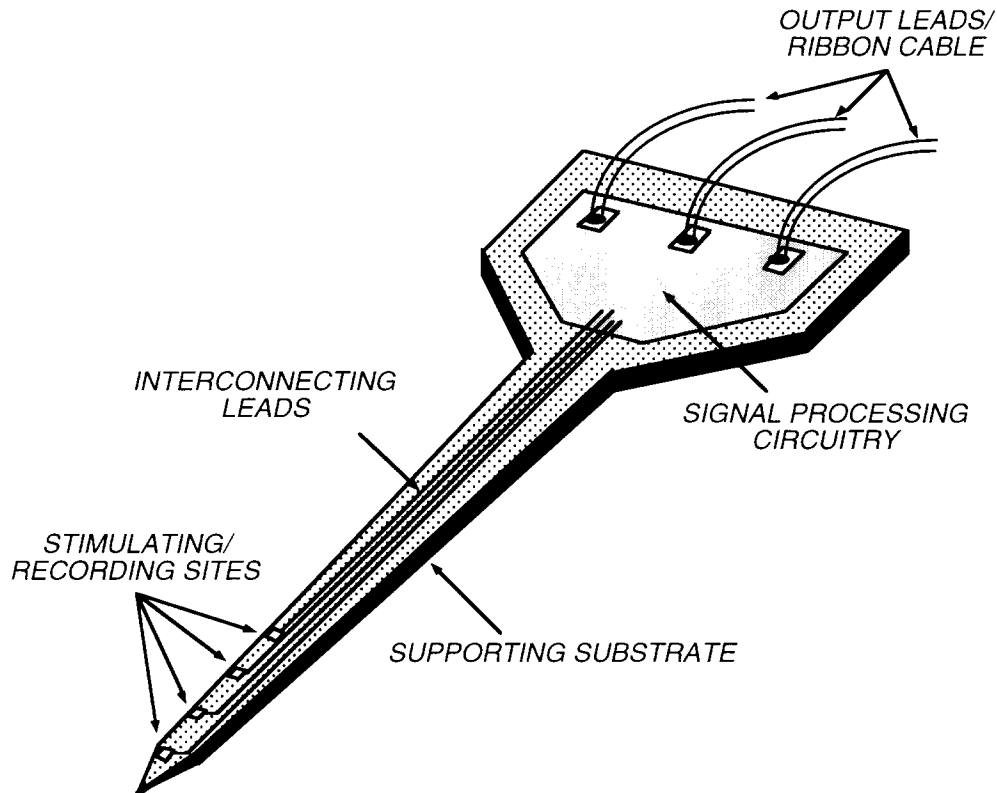


Fig. 1: Basic structure of a micromachined multielectrode probe for stimulating or recording in the central nervous system.

2.1 Basic Probe Fabrication and Site Engineering

On "passive" probes (without any on-chip circuitry), input pads on the rear of the probe body make contact to conductors that lead down the probe shank(s) to electrode sites spaced along the shank(s). Figure 2 shows a photomicrograph of several different probe designs after final etching. Shank widths here are as narrow as $30\mu\text{m}$ with length-to-width aspect ratios of more than 100:1. Approximately 20 different probe designs are included on a typical mask set. Figure 3 shows a close-up of a chronic recording probe, complete with holes in the shank to encourage tissue regrowth and position stabilization. Nearly 100 different stimulating and/or recording probe designs have been produced for investigators nationwide. Nearly 3000 of these probes have been made available through the NCRR-funded Center for Neural Communication Technology at Michigan.

The sequence of steps making up the overall fabrication process for these passive probes is shown in Fig. 4. Fabrication begins with a standard silicon wafer that is oxidized and patterned to define the intended probe areas. These areas are subjected to a deep boron diffusion to heavily dope the probe substrate. The diffusion time and temperature are selected to produce a final probe thickness of about $15\mu\text{m}$. The masking oxide is then stripped and lower dielectric films are deposited using low-pressure chemical vapor deposition (LPCVD). These films consist of a layer of silicon nitride sandwiched between

two layers of silicon dioxide. The thickness of each layer is selected so that the thermal expansion coefficient of the composite insulator matches that of silicon to avoid warp in the final probes. Conductors of phosphorus-doped polysilicon are next deposited and patterned, followed by the deposition of the upper dielectrics, which are identical to those used for the lower composite dielectric film. The upper dielectrics are now patterned using a dry etching process (reactive ion etching (RIE)) to open the stimulating sites and bonding areas. With the masking resist still in place, titanium (300Å) and then iridium (3000Å) are sputtered onto the wafer. The photoresist is then removed, lifting off the metal in all areas except where the upper dielectrics have been opened for the sites and bonding pads. In this most basic process, the iridium sites are thus self-aligned.

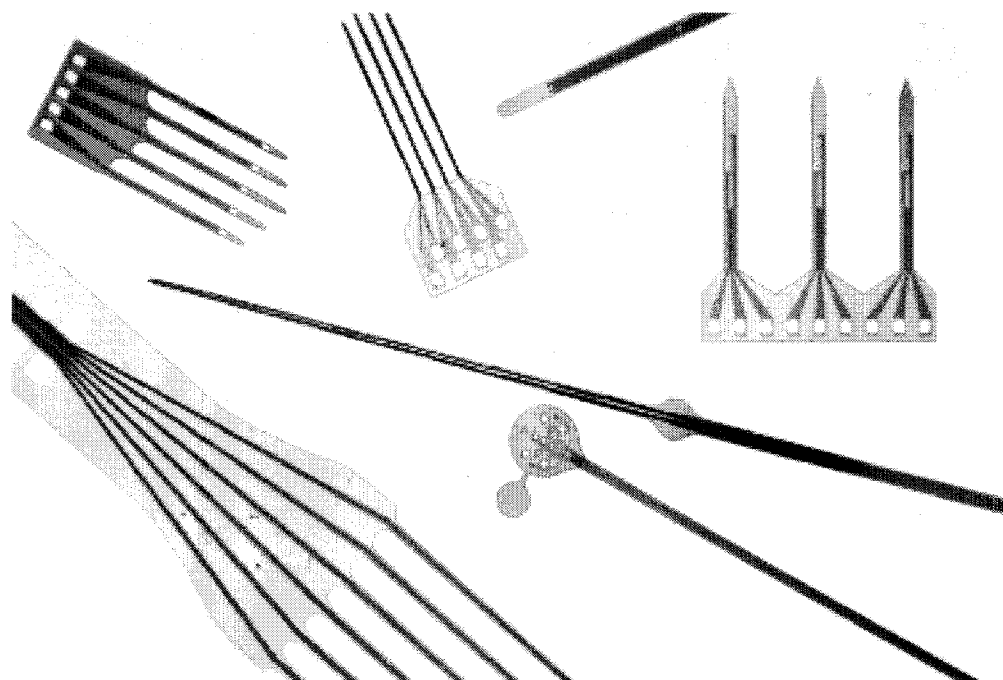


Fig. 2: Examples of a set of probes recently fabricated at Michigan. The probe lengths range from about 3mm to over 18mm. Ribbon cables, which are often built into the probes are as long as 5cm in length. The probes are typically 15 μ m thick with widths from 5 μ m to 80 μ m, depending on the number and size of the sites on the shank.

During the past contract, we have explored the use of alternative interconnect materials for probes and ribbon cables. Polysilicon has a minimum resistance of about 10 Ω /square so that a 5 μ m wide 5mm long lead has a resistance of about 10K Ω , yielding a series voltage drop of 1V for a stimulus current of 100 μ A. This is marginal and should be decreased by about an order of magnitude for use in future stimulating systems. We have explored TiSi refractory interconnects and found them to be acceptable for use in these systems, having resistances of about 1.5 Ω /square. This resistance is stable up to about 800°C; at higher process temperatures, the resistance of the film increases slowly. Thus, it is compatible for use with high-temperature LPCVD silicon nitride but not with LPCVD silicon dioxide (HTO). Tantalum (and tantalum on titanium) films have been found to have a series resistance of about 1 Ω /square in thicknesses of 800nm. While this is rather thick, it is perhaps useable, especially on ribbon cables, and is compatible with low-temperature dielectrics such as low-temperature (425°C) silicon dioxide (LTO) and plasma-enhanced (PECVD) silicon nitride, which are now being used on probes and ribbon cables.

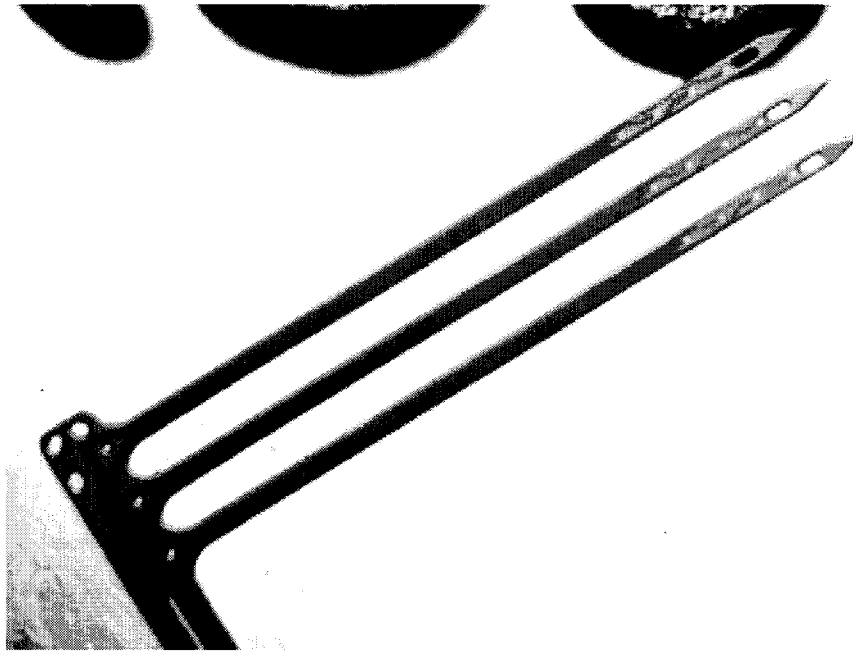


Fig. 3: Close-up of the tip of a chronic three-shank twelve-site recording probe. A ribbon cable exits at right angles to the shank below. Holes are located at several points on the structure to encourage tissue growth and anchoring of the probe position in-vivo. The sites are 100 μ m apart, center to center.

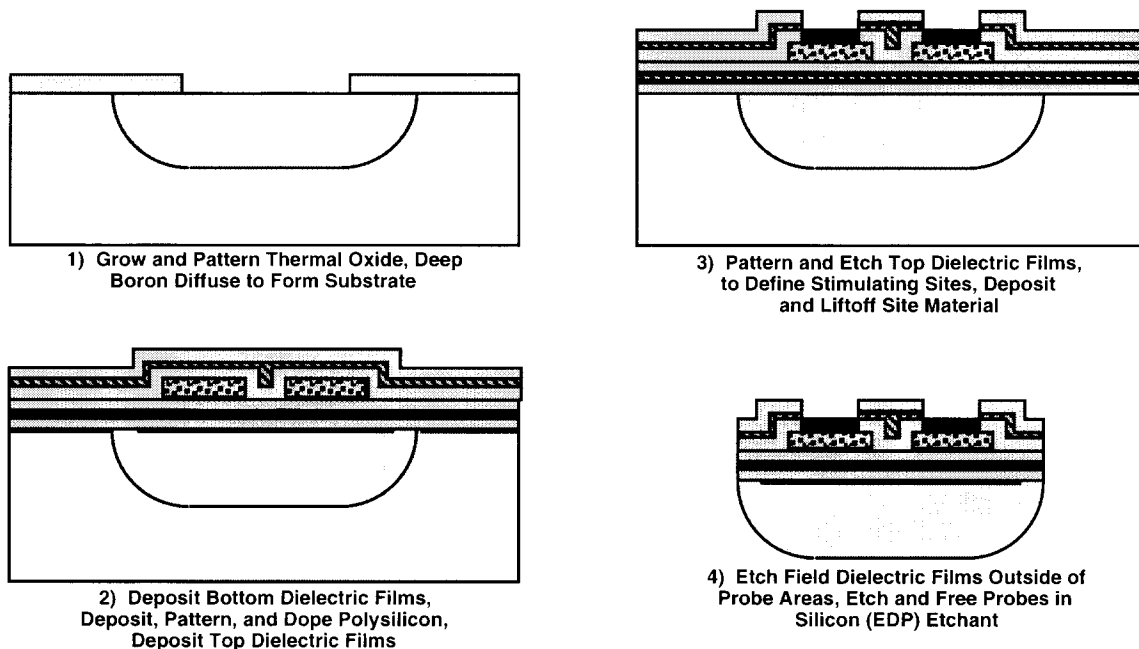


Fig. 4: Process flow for the creation of passive stimulating electrode arrays. The process is single-sided on wafers of normal thickness and requires only four masks when the site material is also used for the pads. The use of gold pads adds a fifth mask. A shallow boron diffusion for sharp tip formation and ribbon-cable definition adds a sixth.

In forming the stimulating sites, care must be taken to ensure that the conductor surfaces in the opened site areas are free of surface contamination in order to ensure that the titanium-iridium site adheres tightly to the underlying conductor. The need to completely remove polymer residue left over from the dry etching step has led to modification of the site formation process mentioned above. Two site processes have been used recently as shown in Fig. 5. In Fig. 5a, a wet etch is used to open the upper oxide layer, followed by a dry etch to open the nitride and expose the lower oxide film. The wafers are then cleaned, and a second (smaller) contact mask is used to open the lower oxide layer. This process results in a tapered contact and also avoids undercutting the nitride layer, which makes step coverage difficult. Finally, titanium and then iridium are deposited and patterned using lift-off. In this case, the iridium site can be substantially larger than the contact via or the conductor, allowing it to overlap adjacent conductors as needed. This saves considerable width on the shanks of stimulating probes.

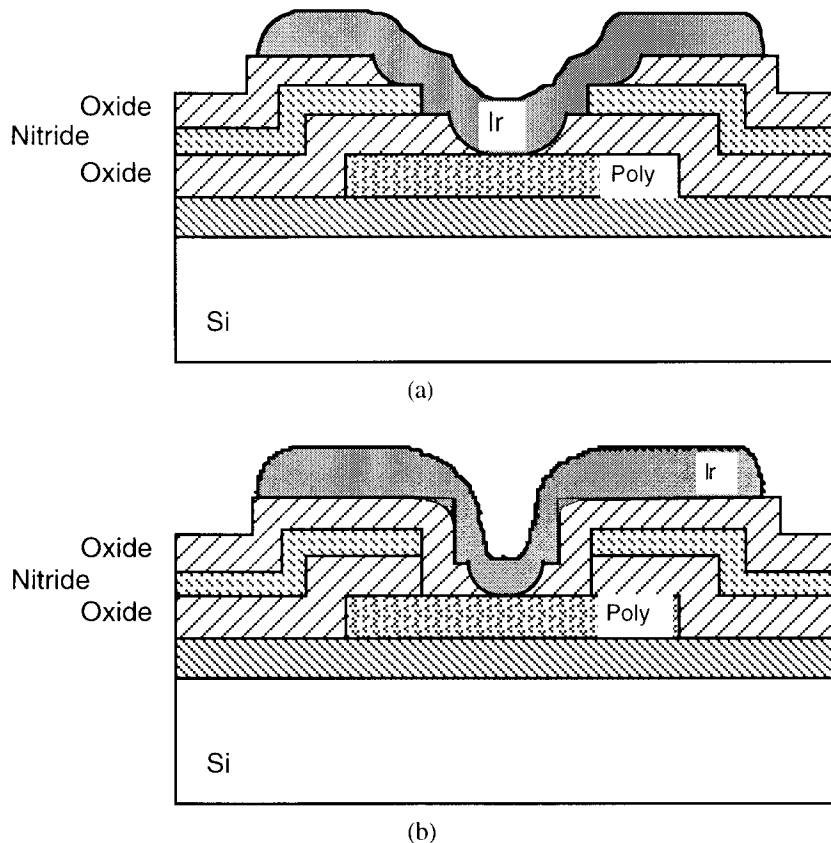


Fig. 5: Cross-section of a three-mask site formation processes. In (a) the upper oxide and nitride layers are opened with a first mask, followed by the opening of the lower oxide with a second mask. The final mask is used for the metal. In (b) the top oxide is not deposited until after the lower oxide and nitride layers have been etched so that the nitride edge is covered by oxide. Both processes ensure a clean polysilicon surface and produce excellent metal adhesion while permitting the metal to overlap adjacent conductors.

In process in Fig. 5b is similar except that the top oxide is not deposited until after the nitride and lower oxide have been opened. This process requires an extra CVD step but results in a covered nitride edge and is now being used for most of our probes. No problems with Ir adhesion or step coverage have been noted with either of these designs.

After site formation using lift-off, gold is inlaid in the bonding sites to allow simple bonding to the probes with either gold or aluminum wire. The field dielectrics outside the intended probe areas are now removed using RIE. Finally, the wafer is thinned to about 100 μm from the back in an isotropic etchant and then subjected to an unmasked etch in ethylene diamine-pyrocatechol-water (EDP) [Seidel 90] to separate the individual probes. The EDP etches silicon but stops on the heavily doped boron regions and does not attack the dielectrics or metals used in this process. The completed probe chips are removed from the etch, ready for lead attachment and mounting.

This passive probe process is capable of high yield, results in very small structures, and requires only single-sided processing on standard silicon wafers. All etching steps are highly selective and self-stopping. Probe features can be controlled to within 1 μm or better. The thicknesses of the finished probes can be varied in the range 1-40 μm by varying the boron diffusion time and temperature and the final etching process [Najafi 90-1, Najafi 85]. The substrate can have any two-dimensional shape as defined by the mask. In addition to the deep boron diffusion for primary substrate definition, a shallow boron diffusion can be added to allow the formation of a sharper probe tip. Such probes enter tissue with very little force and minimal cortical dimpling. Penetration of blood vessels does not result in bleeding but appears to be self-sealing. This diffusion can also be used to form the substrate for an integrated ribbon cable. Such cables are very flexible and using a metal or polysilicon shield are virtually hermetic. They have allowed chronic recording and stimulation over interconnect distances of several centimeters. Figure 6 shows two views of shank tips, illustrating the use of a shallow boron diffusion and the use of an RIE field etch to limit lateral boron diffusion and form a particularly narrow shank.

For acute experimental use, the probe is mounted on a special printed circuit board connector. Electrical connections are made by wire-bonding from the pads on the probe to the connector. This assembly then plugs into a standard dual-in-line-package (DIP) socket to provide easy electrical access to the electrodes. For long-term (chronic) applications, a ribbon cable is typically fabricated as an integral part of the probe, connecting to a Microtech FR-4-12 percutaneous plug. We have considerable experience with this plug but it limits the number of connections in a chronic situation to 12, which is less than we would like. Efforts on high-density chronic connectors are underway both at Michigan and elsewhere. Figure 7 shows an example of one of our present chronic probe assemblies, with the probe, an integral silicon ribbon cable, and the percutaneous plug. The cable connects to the pins on the plug via wire bonds on the lower (implanted) side of the connector.

The ability to form flexible ribbon cables as part of the probe offers one possible means for developing flexible linear electrode arrays for use in a cochlear prosthesis. It represents the first application of silicon microprobe technology to a human prosthetic device, is the largest structure created to date with this technology, and is the first to realize stimulating sites on a flexible substrate. The device is designed to replace the 22-site wire-bundle arrays used in many first-generation commercial implants and opens the way to arrays having many more sites and multiple simultaneously active channels with on-board current generation. The technology offers lower fabrication cost, greater reproducibility, smaller size, a greater number of sites, and embedded positioning features when compared with the wire bundle electrodes now used. Figure 8 shows a photograph of a completed passive prototype array. The device is 46mm long, with an insertable portion that tapers from 640 μm to 320 μm in width over a distance of 25mm. The substrate is formed by a 2.5 μm -thick p++ silicon layer. Site conductors run the full length of the cable in either polysilicon or in tantalum. As in our standard ribbon-cable technology, these leads are insulated above and below using stress-compensated layers of silicon dioxide and silicon nitride.

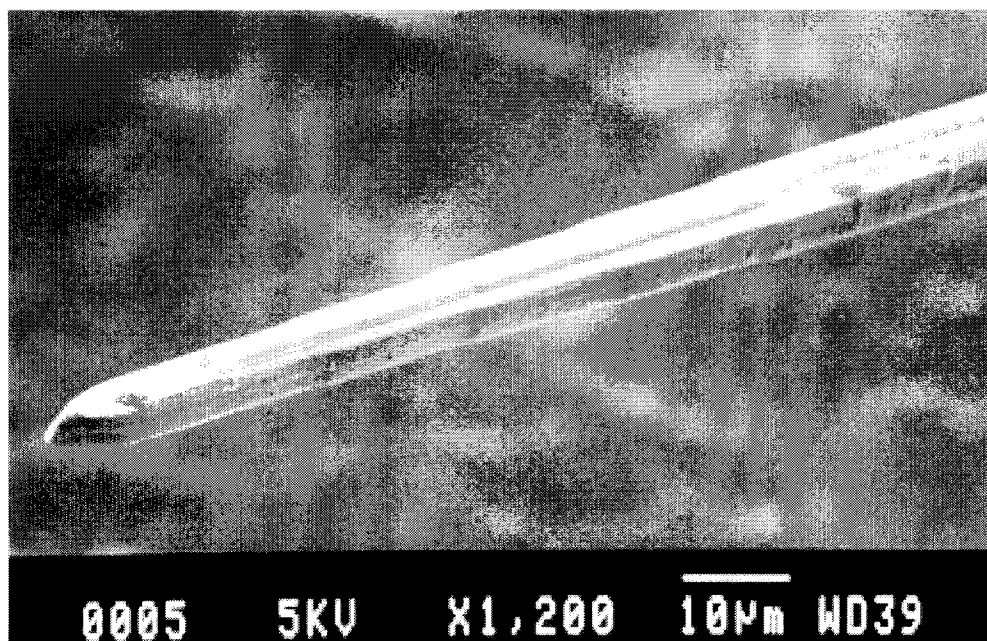
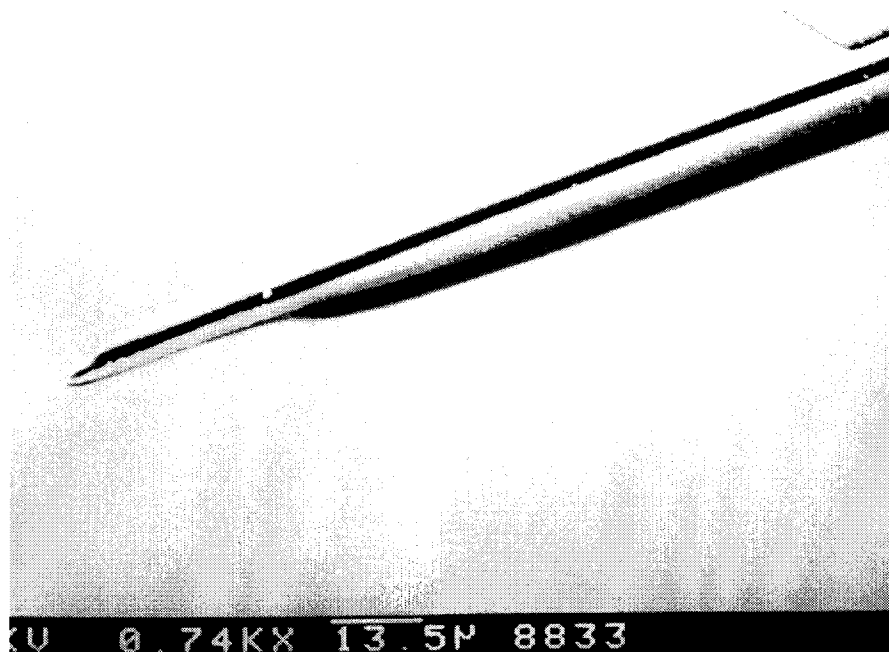


Fig. 6: SEM views of two probe tips. In the photo above, the sharp tip produced using a shallow boron diffusion to complement the deeper diffusion defining the main portion of the shank is shown. An iridium site is located at the upper right. In the photo below, the use of an RIE to limit lateral diffusion and create a narrow shank is illustrated. Two sites are shown.

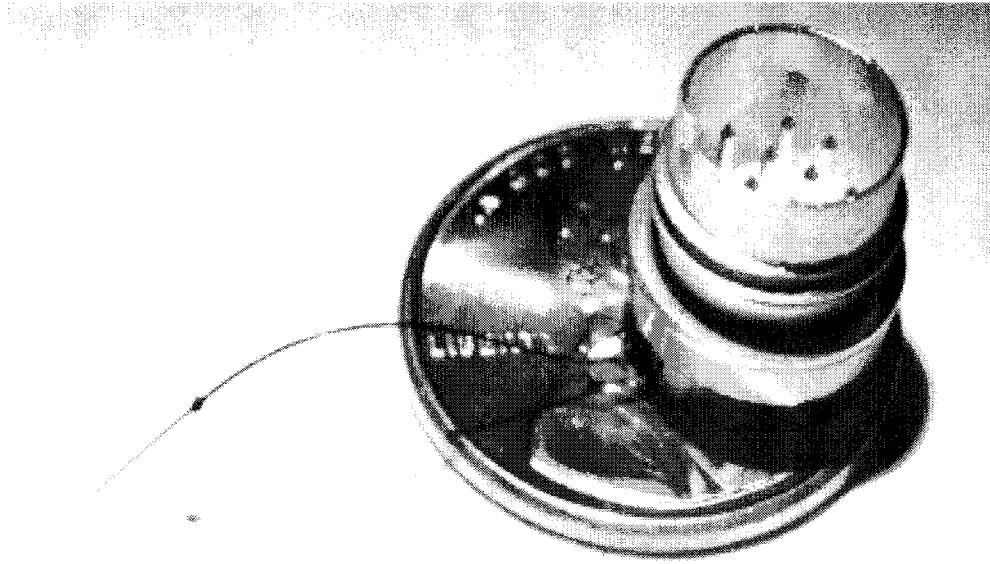


Fig. 7: Photograph of a complete passive probe assembly, including the probe itself, an integral silicon ribbon interconnect cable, and the percutaneous plug.

In Fig. 8, the leads terminate in twenty-two activated iridium (IrO) sites, positioned along the cable on 750 μ m centers. A more recent version, discussed in section 2.3 below, increases the number of sites to thirty-two and adds distributed multiplexing circuitry along the cable. The sites are 250 μ m in diameter and overlay the interconnects. The entire array is insulated with deposited parylene, which is laser-ablated to expose the sites. Tests have shown that laser ablation, followed by an oxygen plasma to remove residual polymer from the sites, results in normal impedance characteristics for stimulating sites. The parylene provides the primary strength to the cable and is conformal. The cable is slit at regular intervals to increase flexibility and firmly anchor the parylene to the probe.

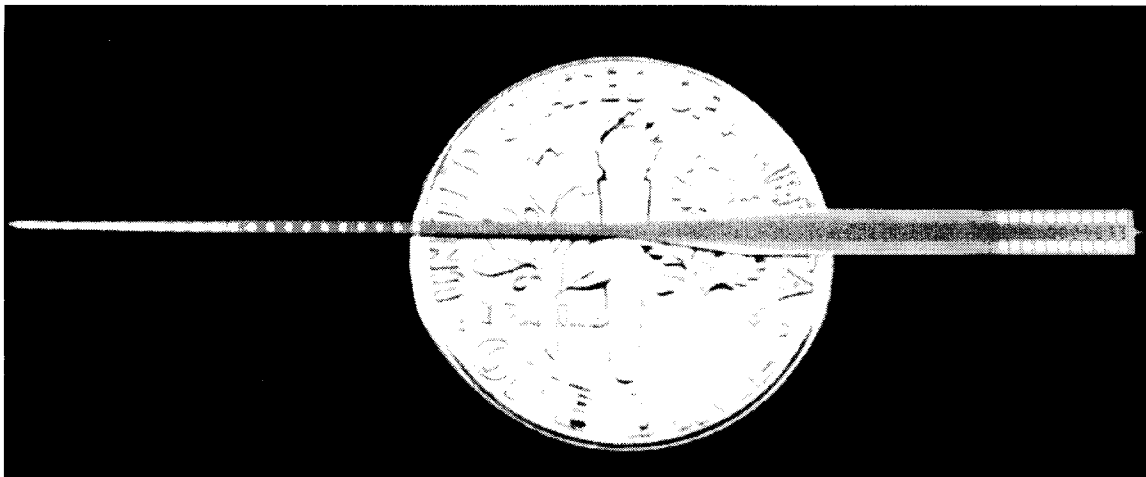


Fig. 8: Top view of a 46mm-long flexible probe for a cochlear prosthesis. On this probe a total of 22 sites are distributed over the 25mm-long insertable portion of the probe. The probe is insulated with an overcoat of parylene which is removed from the sites with laser ablation. This application may mark the first application of the probe technology to a neural prosthesis for human use.

In order to implant the device, the tapered end-section of the array is inserted through the round window into the spiral cochlea of the inner ear. In inserting such devices, it is very important to position the device carefully so that it hugs the inner diameter of the cochlea in order to achieve good neuronal coupling. The cables can be pre-bent before parylene deposition to mimic the required shape when inserted. In addition, an array of polysilicon strain gauges is being integrated on the cables to allow imaging of the array shape/position during and after insertion. It appears it will be possible to resolve bending displacement changes (the position of the cable in the cochlea) of 50 μ m or less at the end of the 25mm cable. The outputs from eight segmented strain gauges along the probe are used externally to generate and display a smoothed image of the array shape. These arrays have been inserted into a human cadaver cochlea, verifying the ability to position them so that they conform to the shape of the canal. At a current of 300 μ A, the in-vitro compliance voltage is about 0.5V using tantalum leads.

It should also be noted that we are beginning to explore titanium nitride as an alternative to activated iridium as a site material. Titanium nitride is used extensively as a contact barrier material in integrated circuits and so is commonly available in most IC foundries as well as in our Laboratory. It is used as a passive barrier in the circuit contacts of all of our active probes. The German group at Reutlingen has reported that while the charge capacity is less for TiN than for activated IrO, the charge delivery capability is somewhat greater (perhaps by a factor of more than three). We are working to confirm this experimentally. Probes have been fabricated using TiN sites, establishing that TiN is compatible with our overall probe process. The etch rate for the material in EDP during wafer dissolution is less than 2nm/min, which is acceptable. Although the Reutlingen group has indicated that the material must be deposited at low angles of incidence, we are exploring normal incidence as well. Sites deposited using TiN sputtered at normal incidence appear to have impedance levels as low as those of activated IrO. This is encouraging since maintaining IrO sites while probes are in storage is uncertain and TiN is more compatible with eventual foundry fabrication. Frequency spectroscopy, pulse tests, and cyclic voltammetry tests are on-going with these sites. Figure 9 shows the top view of a TiN site deposited at normal sputtering incidence. The film is columnar in nature and its high porosity may explain its low impedance characteristics. Its stability and biocompatibility at high current levels must still be confirmed.

2.2 Three-Dimensional Microelectrode Arrays

Since the structure and process used for our electrode arrays is inherently planar, one- and two-dimensional arrays are easily realized; however, neural systems are three-dimensional, and thus for any practical prosthetic device it is of interest to be able to define three-dimensional stimulating arrays in order to fully instrument the target tissue volume. This requires a method for assembling several planar probes to create the needed structure. The structure we have adopted is shown in Fig. 10 and has been successfully used with both recording and stimulating arrays. It is based on inserting several probes in a platform that rides on the cortical surface. Spacers are inserted to hold the probes parallel, while gold lead tabs on the probes are bent at right angles and are bonded to pads on the platform.

As the probes are inserted in the platform, the platform is held around its rim to provide a solid bonding base. The gold beam tabs are bent at right angles using a special micromachined jig as shown in Fig. 11. The "wings" containing these lead transfers have a low profile to allow an ultrasonic bonding tip to contact the pads and effect the bond [Bai 96]. Four-probe 3D arrays can be assembled in about 20 minutes and have been used in many acute experiments to date.

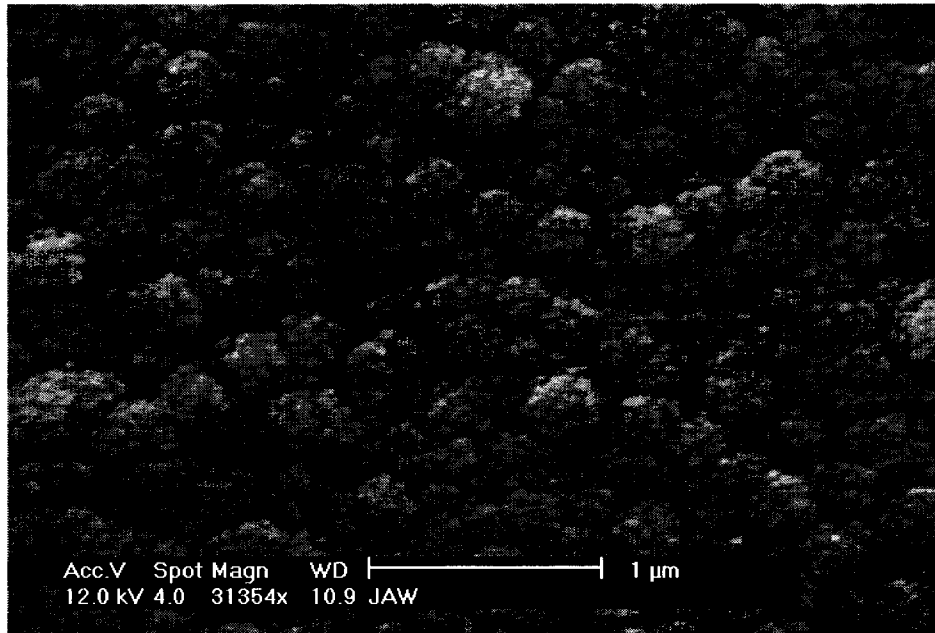


Fig. 9: Top view of the typical columnar structure of TiN sputtered at high pressure and normal incidence.

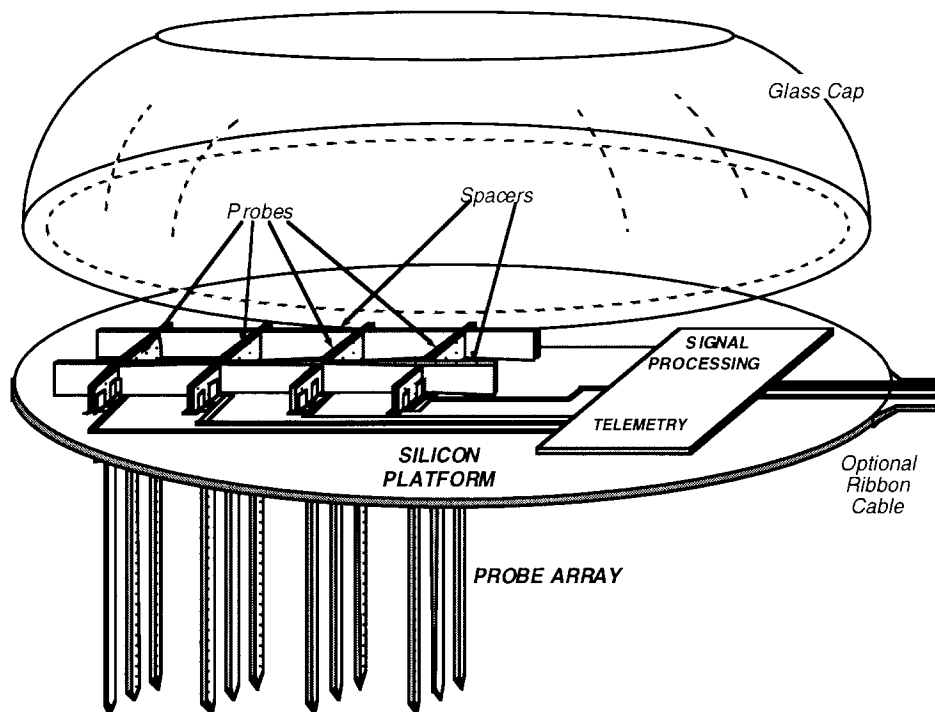


Fig. 10: Overall view of a three-dimensional multi-probe microassembly. The platform rides on the cortical surface and beam leads on the probes provide lead transfers to the platform. Output connection is provided by either platform-mounted telemetry or a hardwired ribbon cable and percutaneous plug.

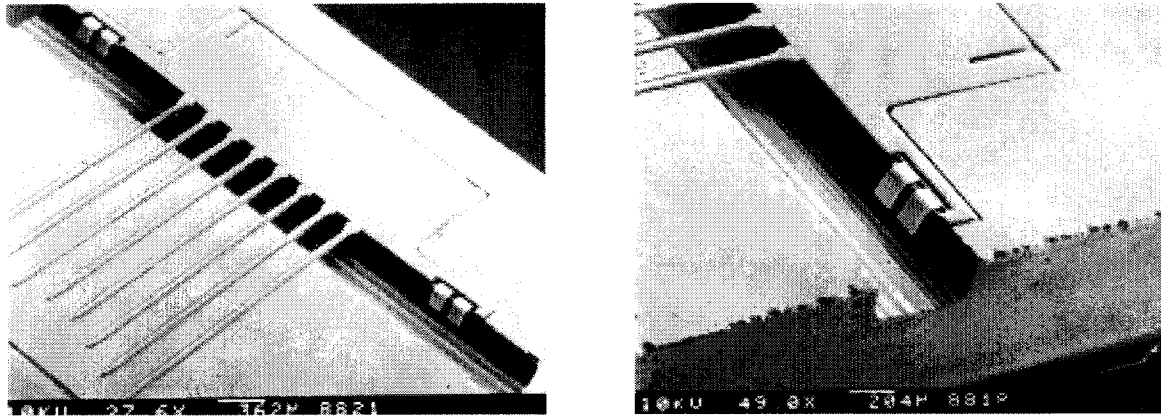


Fig. 11: View of a 3D probe held in a micromachined jig used to bend the lead transfers prior to insertion in the platform.

Figure 12 shows the bottom side of an array of eight 16-shank probes with shanks on 200 μ m centers. Although the array looks formidable, the shanks are quite thin so that the tissue displacement by such an array is still less than two percent. A stimulating array would have a shank spacing of 400 μ m, reducing the displacement further. Having so many shanks is a significant help in anchoring the probes in tissue; however, inserting them without excessive cortical dimpling is a challenge. While individual probes penetrate the pia arachnoid easily in rats, guinea pigs, and cats, larger arrays are more difficult to insert. Microassemblies such as those in Fig. 12 can be placed in guinea pig cortex with minimal cortical dimpling, but in cat the shanks simply bend without penetrating. Accordingly, we have developed a dynamic spring-loaded insertion technique similar to that reported by the University of Utah [Rousche-92]. The probe array is held by vacuum and positioned over the cortex. When fired, the throw of the tool is adjustable over the range of a few millimeters and the insertion speed is adjusted using different stiffness springs. Typical insertion rates are in the range of 20-100cm/sec. The inertia of the brain and the pial surface makes movement there impossible and penetration is achieved with minimal dimpling. Histological studies to determine the degree of damage along the probe tracks are still on-going, but results thus far are encouraging so long as the probe shanks are carefully aligned with the direction of insertion. Other studies have shown that it is important to limit the probe rise above the platform to ≤ 1 mm in chronic implants to avoid any anchoring of the implant to the skull, which creates mechanical tissue irritation near the probe tips as the brain moves with respect to the skull.

2.3 A Sacrificial Bulk Micromachining Technology for Probe Substrate Definition

During this past contract, we have explored several process alternatives for use in defining the probe substrate to see whether they might offer significant advantages over the boron-diffusions that have become traditional in this role. The boron diffusion step is the least foundry compatible of all those used for probe fabrication. Even though it is offered commercially by some MEMS foundries, it is not commonly found in integrated circuit process facilities. The approach explored initially as an alternative to boron used a porous silicon layer, formed by electrochemically etching a p+ buried sacrificial silicon layer, to allow release of the probe structure without etching through the entire wafer. This release can be performed at room temperature, where the silicon etch does not significantly attack

even exposed aluminum. More recently, we have found that the use of an arsenic-doped n+ buried layer is preferable for defining the substrate. This step avoids the outdiffusion problems associated with a p+ buried layer and avoids having to process the silicon after porous layer formation. Instead, an arsenic-doped buried layer is formed in the probe substrate early in the process. Arsenic has a much lower diffusion coefficient than boron and does not move significantly during subsequent processing. Epitaxial growth, planarization using a chemical-mechanical polish (CMP) (available commercially), and circuit fabrication then take place. After metallization and site formation, the probe is masked and subjected to a biased electropolishing etch in HF, which selectively removes the buried layer, releasing the probe from the wafer. This process is simpler than the process involving porous silicon; however, the release etch in HF is more difficult to mask than the porous silicon etch and requires that the probe area be capped with nitride and an appropriate HF mask. RIE is used to define the lateral extent of the probes. With either the p+ porous or the n+ electropolishing process, avoiding the long through-wafer etch is increasingly attractive as wafer sizes, and thicknesses, increase.

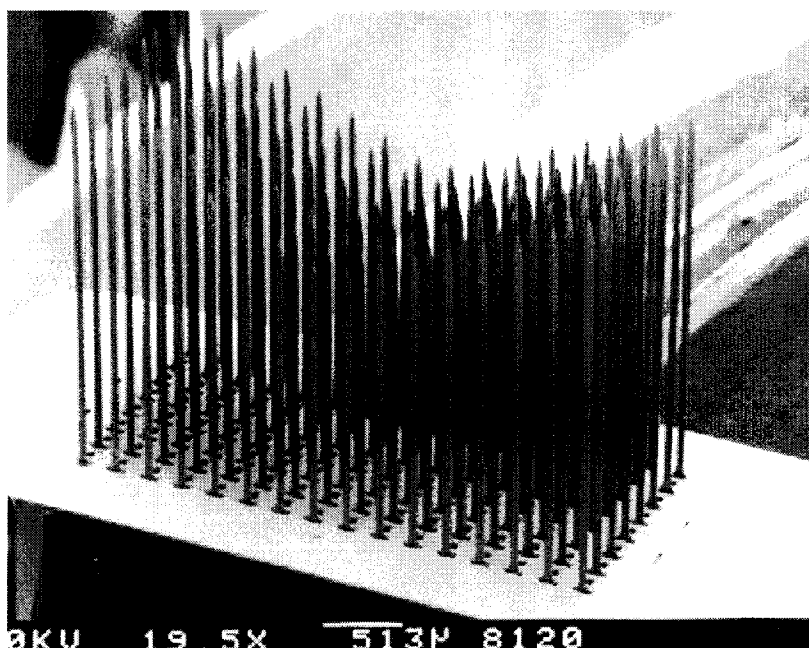


Fig. 12: SEM view of the shanks of an array of eight 16-shank neural probes using the microassembly approach shown in Fig. 8. The shanks here are on 200 μ m centers.

We have now completed our look at these alternative processes. As an application vehicle, a mask set which included 32-site active cochlear stimulating probes and 5-site passive recording probes was used. The cochlear probe was designed to allow stimulation of four channels simultaneously. Site selection is performed on-board, while the currents are generated externally. A series of eight polysilicon strain gauges, noted above, were placed on the front-end insertable portion of the implant to measure bending of the substrate during and after insertion into the spiral cochlea. One of the eight gauges is selected at a time and its output compared differentially with a back-end reference resistor. Readings from the eight gauges can be used to form an image of the implanted substrate, allowing stimulus current levels to be adjusted for varying position in the cochlea. The general shape of the probe is similar to that of the probe shown in Fig. 8. Figure 13 shows device cross-section, indicating its general process and structure.

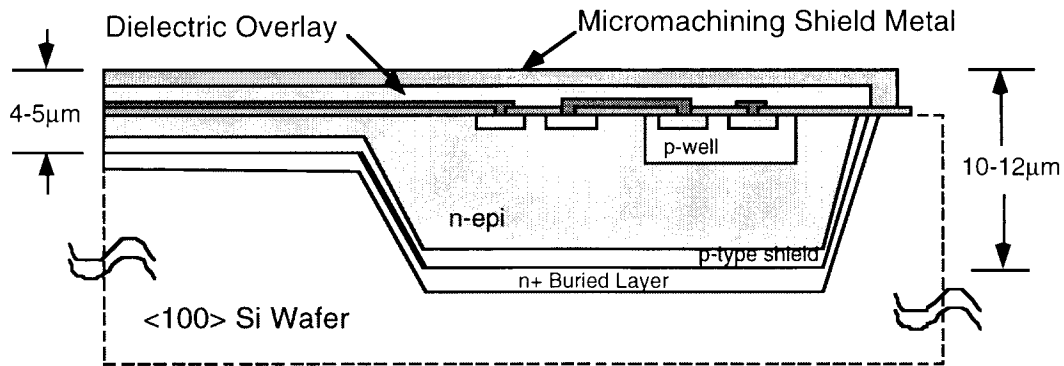


Fig. 13: Cross-section of a portion of a cochlear ribbon probe, used as a vehicle for exploring the use of an n+ buried sacrificial layer for probe release from the wafer. At the end of the process, the n+ layer is etched away, freeing the probe. The micromachining shield is then subsequently removed.

In fabrication, the substrate is first recessed to set the desired depths of the ribbon-cable sections and the circuit islands. Since the n+ buried layer process retains lightly-doped silicon for the probe shanks and circuit islands, demultiplexing circuitry can be distributed down the “shank” of the probe, reducing the number of leads required and, for a given width, allowing wider conductors and lower end-to-end interconnect resistances. After recessing the substrate, epitaxial silicon is deposited and planarized using CMP. The circuit process is executed followed by interconnect metal and site formation. Finally, the wafer is biased and placed in an HF etch to selectively undercut the buried layer. An example of the ability to undercut such a sacrificial buried layer is shown in Fig. 14.

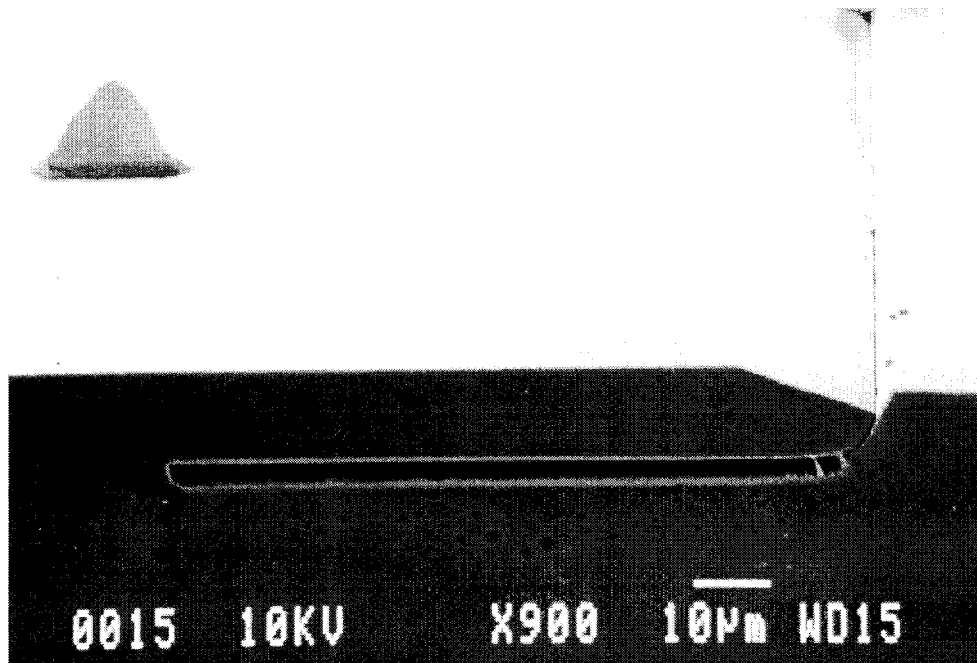


Fig. 14: Cross-section of an n+ buried layer under an epitaxial silicon region. The buried layer has been partially removed, illustrating the ability of a biased etch to selectively undercut a probe from the front of the wafer.

Figure 15 shows a top view of the circuitry on one of the distributed circuit islands. This circuitry was fully functional. The only difficulties in the processing sequence were during the final release etch, where masking the HF was expected to be problematic. Our experiments have shown the ability to etch $1\mu\text{m}$ -thick n^+ layers laterally at rates exceeding $10\mu\text{m}/\text{min}$. Metal masks have been sufficient to protect the devices while undercutting lateral structures up to $500\mu\text{m}$ wide (from both sides); however, longer distances (etch times) resulted in excessive lifting of the Cr-Au mask. This performance is sufficient to undercut most ribbon-cable structures but is not sufficient to undercut the $640\mu\text{m}$ -wide cochlear probe completely. However, using etch-access slits (commonly used for enhanced flexibility on ribbon cables) at $200\text{--}300\mu\text{m}$ intervals, undercutting should be readily accomplished. We suspect that part of the etch-mask problems have come from the fact that when the metal etch mask overlaps the silicon substrate, it becomes biased, enhancing attack of the chromium layer under the gold. If the mask is arranged so that it remains on top of the dielectric, we expect masking will be less of a problem.

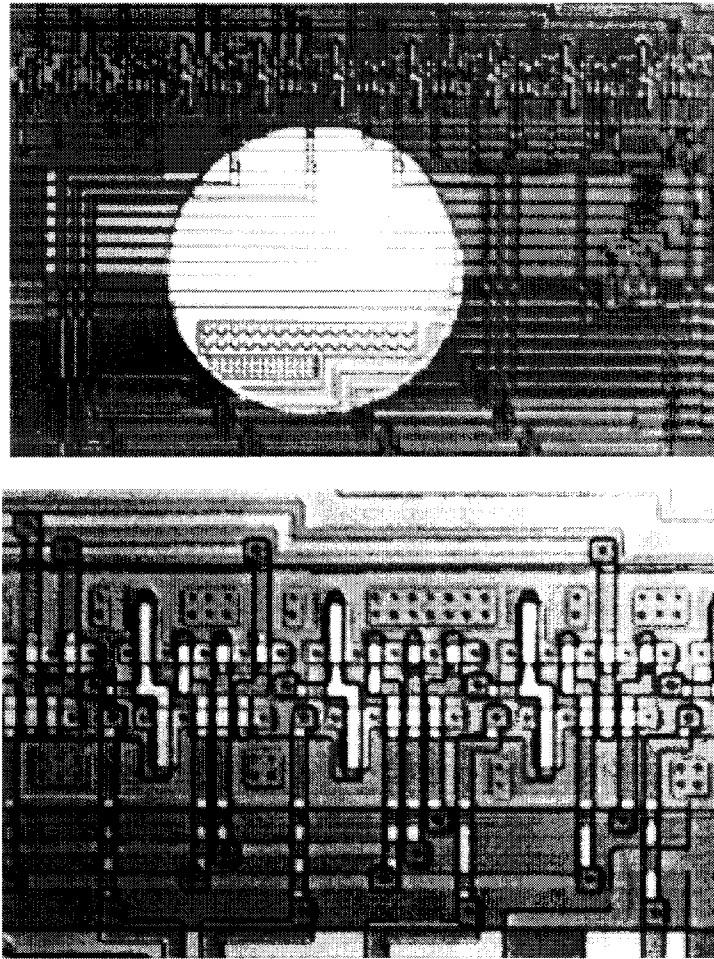


Fig. 15: Top view of the circuitry on a 32-site cochlear probe test vehicle. The top photo shows a view of the demultiplexing circuitry on one circuit island on the ribbon-cable probe along with a $250\mu\text{m}$ -diameter stimulating site. The lower photo shows a closeup of the demultiplexing circuitry.

Our conclusion from this study is that an n^+ buried layer can be used as a bulk sacrificial layer for front-side probe release. The process offers several advantages.

Unlike the current boron process, it provides an etch-stop on all sides of circuit areas and, as a result, totally eliminates etch timing in release of the probes from the host wafer. It would also allow some circuitry to be moved from the back end of the probe to the shanks, decreasing the back end profile and enabling the number of sites to be increased without the number of leads increasing proportionally. This is especially important in devices such as the 4.6cm-long cochlear implant probes, where wide leads are desirable to reduce voltage drops along the current lines. It also uses processes that are foundry standard (epi growth, CMP) and foundry compatible (electropolishing in HF) for the micromachining steps. However, the new buried-layer process is more complex than the boron etch-stop currently used, and the epitaxial and CMP steps required are not currently available in our laboratory. In addition, the highly-doped boron substrate has other advantages. It also provides an etch stop to prevent the slow attack of the silicon substrate by biological fluids (saline) and reduces the minority-carrier diffusion length in the substrate to significantly reduce optically-generated noise and offsets. Further, it virtually eliminates the surface depletion layer in the substrate increasing the coupling capacitance to the extracellular fluid and lowering the bulk resistance of the substrate to suppress crosstalk. Thus, we have no plans to switch to the buried layer process at this time but will keep it in reserve to be used as needed in the future. Some work will continue under other funding to explore this process further for a cochlear probe, where it is especially advantageous, and if the masking problems can be convincingly eliminated its use for CNS penetrating electrodes may be revisited in the future.

In summary, in the area of passive stimulating probes, we have continued to fabricate a variety of probe designs for internal and external users. These have included a flexible 22-site array for potential use in a cochlear prosthesis. It has been feasible to insulate this probe with parylene and subsequently expose the sites using laser ablation followed by an oxygen plasma to remove residual polymer. Site designs have evolved to a three-mask process that ensures good site adhesion and adequate step coverage. Both titanium silicide and tantalum have been explored as alternatives to polysilicon for probe interconnect. They are process compatible and capable of reducing the end-to-end resistances of the lines by as much as an order of magnitude. Titanium nitride is being explored as an alternative to IrO as a site material with encouraging results to date. Finally, we have explored alternatives to the boron etch-stop for substrate formation. While the use of a buried n+ sacrificial layer allows the formation of circuitry along the probe shanks and permits the final probe release etch to occur at room temperature, this process is more complex than the boron process, which also provides a highly doped substrate to suppress crosstalk and other noise sources. Thus, we have a high degree of confidence that our present process is optimum for probe fabrication. The following sections describe the fabrication of circuitry on the probes, which is essential to allow many sites to be controlled from a small number of external leads. Indeed, active probe fabrication was the central focus of the past contract.

3. Active Stimulating Arrays: Basic Design and Fabrication

The driving force behind the integration of electronics on the probe substrate is the desire to limit the number of output leads to a small number (e.g., five) while permitting the use of many different sites for high spatial selectivity. A small number of external leads is essential for two reasons. First, it is difficult to attach very many leads to a probe only a few millimeters across, and this part of the process is a one-at-a-time enterprise that is labor intensive. Second, when attached, the leads impose a stiffness and tethering on the probe that makes implantation difficult and can induce migration in long-term implant situations. For a stimulating probe, the goal is a circuit block that can accept serial data from the outside world and will then generate, on-chip, the required currents for each of the addressed sites. This implies a digital-to-analog converter (DAC) per active site, and that converter must be capable of biphasic current drive. It is generally felt that such a device should have 8-bit biphasic resolution over a current range of at least $\pm 100\mu\text{A}$ and perhaps as great as $\pm 254\mu\text{A}$. We have elected to keep virtually all timing external in order to minimize the complexity of the probe itself, i.e., currents are started and stopped on external command with no timing performed on the probe. It is also clear, however, that there must be a variety of safety checks to protect against malfunctions that could damage the surrounding tissue.

Figure 16 shows the general block diagram of the active probe electronics. An external system maintains a buffer memory loaded with the code sequences needed to launch the intended current patterns from the probe at the proper times. The control system writes this data to the probe over a serial data line. Synchronization is maintained using a separate clock line, and since the probe is to deliver biphasic currents, positive (VDD) and negative (VSS) supplies are required. This implies a five-line system so long as on-chip current generation is used. The data word consists of an address followed by data which sets the amplitude of the intended current pulse. The address and data are latched, and the new current pattern from the probe is initiated. This current pattern, in principle, will be maintained until altered by the external control.

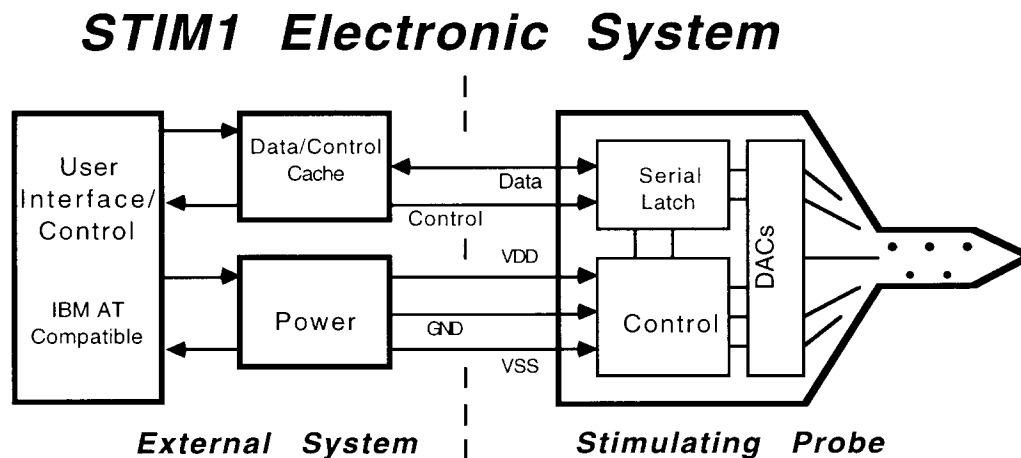


Fig. 16: Overall block diagram of an active stimulating probe.

We have designed a series of active probes, differing in complexity, the number of active channels, the total number of sites, and the number of on-chip features as follows:

- STIM-1b:** A monopolar active stimulating probe with 16 sites. An externally-generated stimulating current is steered to a site selected by a serial input address. Only one site is active (driven) at any one time. Power-on reset and parallel site activation modes. Development of this probe is completed; it is fully operational and has been demonstrated in-vivo.
- STIM-1a:** A bipolar active probe with 16 sites and on-chip current generation. A serial input data word selects two of 16 sites and a stimulus current amplitude. The current is generated and applied to the first site and is mirrored and applied to the second site. Thus, two sites can be active at any time. Power-on reset and parallel site activation modes. Development of this probe is completed; it is fully operational and has been demonstrated in-vivo.
- STIM-1:** A 16-site active stimulating probe with on-chip current generation. The serial data word selects one of 16 sites and the desired current amplitude (0 to $\pm 256\mu\text{A} \pm 2\mu\text{A}$). All 16 sites can be simultaneously active. Power-on reset, parallel activation, site impedance test, anodic bias, and current calibrate modes along with per-channel pulse time-outs and per-frame operation checks. This probe was the basis for STIM-2 below. [Tanghe 92-1]
- STIM-2B/-3B:** This is a 64-site, four-channel active stimulating probe with off-chip current generation. A static analog multiplexer is used to select four of the 64 sites under the influence of a serial address stream (as four 1 of 16 selects). Externally generated currents are then directed to these sites. Power-on reset and parallel site activation modes. External impedance testing. Any selected site can be set for either stimulation or recording. STIM-3B is a three-dimensional (3D) version of STIM-2B (2D) with provision for multi-probe platform mounting. This probe was developed under the past contract and is now being used in-vivo. It is fully operational.
- STIM-2:** This is a 64-site eight-channel active stimulating probe with on-chip current generation. A front-end channel selector selects 8 of the 64 sites under the control of a serial input bit stream. Each data word sets the address (one of eight) of a desired site and the stimulus current amplitude to be applied (0 to $\pm 127\mu\text{A} \pm 1\mu\text{A}$). Eight channels can be simultaneously active. Modes: low-impedance shunt mode for idle sites, anodic-bias mode, electrode-impedance monitoring mode, electrode recording mode, self-test and trouble flag modes, and electrode-activation mode. This probe has been sampled [Kim 96] and its design was iterated during the past contract. Its fabrication was deferred until STIM-2B was operational since that probe offered a simpler vehicle for completing process development.

STIM-2B/-3B and STIM-2 were major focuses for work under this contract and will be discussed in sections 4 and 5 of this report. However, first, the fabrication process for integrating circuitry on the probes will be discussed. The development of a high-yield active probe process has required considerable effort, especially in the areas of contacts, encapsulation, and micromachining. Recent advances in these areas have resulted in a stable high-yield technology base which will be central to all future probe fabrication, as discussed in the paragraphs below.

Figure 17 shows a perspective view of the active probe structure along with a longitudinal cross-section. It is similar to the passive structure except for the inclusion of CMOS signal processing circuitry. Since the probe shanks are in direct contact with the tissue, they must be grounded. To provide electrical isolation between the circuitry and the tissue, an n/p p-well epi-CMOS technology is used. A p-tub is formed around the circuit areas using a combination of the deep-boron areas (p++) and the p-type substrate under the circuitry. The probe shank and p-tub are grounded, providing the necessary electrical isolation from the n-bulk region, which operates at +5V when the circuit is powered. Note that the use of an electrochemical etch-stop on n-type material is probably precluded here since the exposed substrate must be p-type and must be grounded.

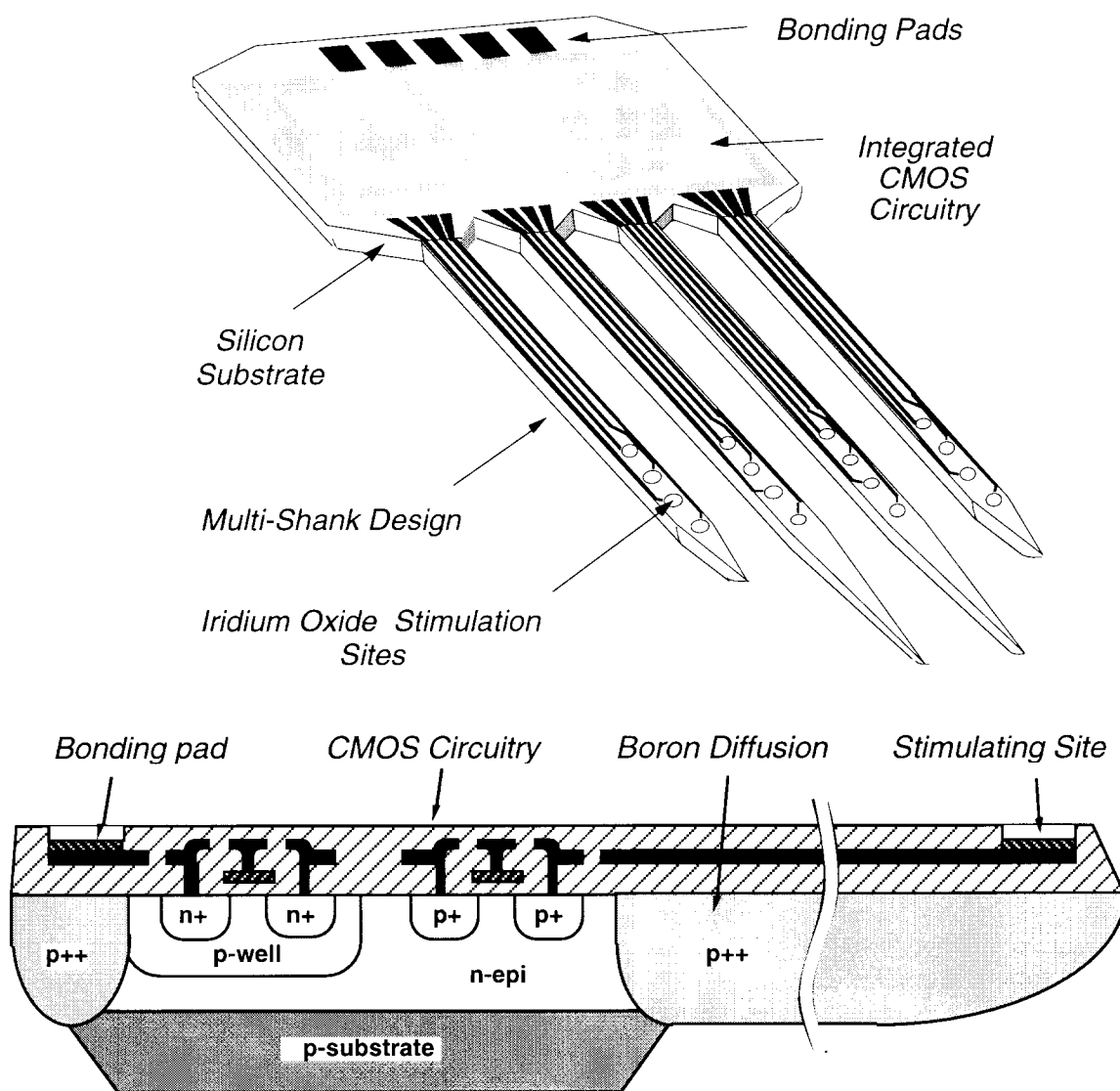


Fig. 17: Perspective view and longitudinal cross-section of an active stimulating probe.

The fabrication procedure is very similar to a standard CMOS integrated circuit fabrication sequence with steps added to form the probe and the electrode sites. Fabrication starts with a standard p-type silicon wafer that has an n-type epitaxial layer on the surface

that is 15 μ m thick. The p-wells for the circuitry are implanted, followed by the deep boron diffusion to form the intended probe shapes. During this diffusion, the p-wells are driven in to a depth compatible with the circuit process. Next, standard CMOS circuit fabrication takes place through metallization to form the circuitry on the probe. Upper dielectrics are deposited to provide insulation for the circuitry and are opened in the areas where the sites and bonding pads are located. These sites and pads are formed by depositing and lifting off iridium, as in the passive process. Finally, the wafers are thinned from the back and etched in EDP to separate the completed probes.

There are three main differences in the circuit fabrication part of this device that are not standard in CMOS circuit fabrication [Ji 90, Lund 94, Bai 98]. First, the p-well drive-in and the deep boron etch-stop diffusions are performed simultaneously. This requires adjustment of the p-well implant dose and energy to compensate for the additional masking oxide needed to protect the p-well from the deep boron diffusion and for segregation of the implanted boron into this oxide. A portion of the deep boron drive-in can be performed prior to the p-well implant to allow independent optimization of the p-well junction depth and the shank thickness [Kim 96]. Secondly, special dielectrics are required over the shank and circuit areas to protect the probe from the cellular environment. Finally, special precautions must be taken to ensure a sufficiently wide process window to retain the p-substrate in the circuit areas of the probe, since no etch-stop exists in this area.

For the active probes now being fabricated, the structure shown in Fig. 18 is used over the circuit areas. Aluminum interconnects are used over the circuit area and are covered with low-temperature CVD oxide (LTO). These materials are deposited after high-temperature LPCVD dielectrics are deposited on the shanks over polysilicon interconnects. This allows the highest quality dielectrics on the shanks but maintains a standard interconnect-dielectric sequence over the circuit block. Titanium plugs are used in the circuit contacts to prevent junction spiking. In addition, since the LTO layer is very thick (1.2 μ m), titanium is interleaved with several layers of aluminum to form the metallization as a multi-layer stack and ensure freedom from hillocking. A PECVD nitride layer can be added over the LTO as an option. After the sites are opened and the pads have been inlaid, a metal barrier can be added over the circuit area along with a polymeric film. Thus, the LTO is not exposed to the external fluid, and the circuit area, which is segregated at the rear of the probe, can be coated with additional barriers to prevent degradation in-vivo. Such polymeric films are used over the rear areas of many 2D chronic probes to provide a handling base, and the rear areas of 3D platform-mounted probes are potted in polymer.

The final challenge is to protect the rear areas of the probes so that the shank areas are released during the wafer dissolution step well before the back areas, which must retain a thick p-region under the circuit areas without an etch-stop. Dielectric corner compensation (dielectric bridges into the field areas) prevent undercutting at the outside corners of the circuit areas, but with the shanks aligned along the $\langle 110 \rangle$ directions, the probe shanks do not undercut from the front but rather etch back from their tips. This makes it difficult to release the shanks and 3D mounting wings without compromising the substrate material under the circuitry. However, using a RIE to deep-etch around the shanks and the wings from the front prior to the wafer dissolution etch allows the shanks to etch laterally, releasing them well before the back-etch reaches the circuit areas. Thus, at least 100 μ m of p-type silicon can be retained and any critical timing of the dissolution etch is avoided. Figure 19 shows a top view and diagram of this etching arrangement while Fig. 20 shows photographs of these deep RIE (DRIE) slots around a 3D probe.

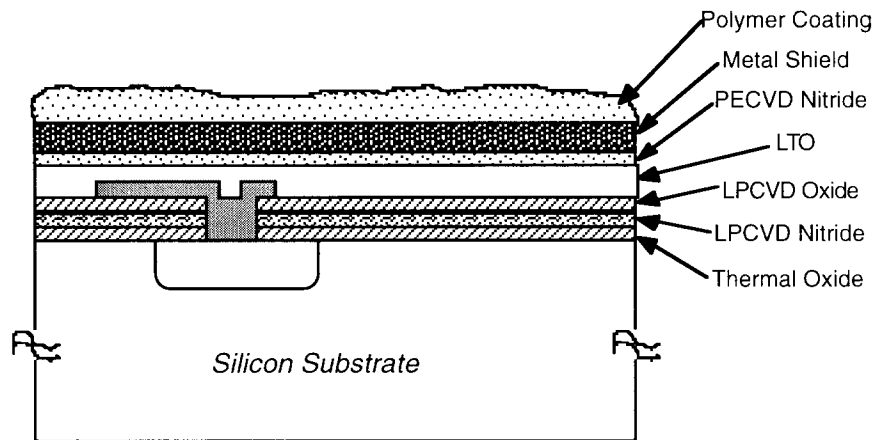


Fig. 18: Cross-section of an active probe and the upper dielectric layers. Polysilicon interconnect is used on the probe shank buried under high-temperature dielectrics. Aluminum interconnects are used over the circuit area (lower figure) covered by LTO, PECVD nitride, a metal shield, and a polymer.

4. STIM-2B/3B: A Multiplexed 4-Channel 64-Site Probe with Off-Chip Current Generation

STIM-2B (or “QuadraStim-EX”) was developed during the past contract as an intermediate-complexity active stimulating probe. This probe has 64 sites with on-chip multiplexing to steer each of four independent externally-generated stimulus currents to one of 16 stimulation sites. The four channels are each capable of providing $\pm 100\mu\text{A}$ to the tissue or can be used for recording if desired. A three-dimensional version of this probe (STIM-3B) has also been realized by making the necessary structural modifications to allow platform mounting and making some changes to the electronics to allow addressing multiple probes in a single array. Table 1 summarizes the specifications and special features for this probe.

The overall system architecture of STIM-2B is shown in Fig. 21. The probe utilizes a 20b shift register to load four 4b addresses which are decoded by a NAND-type decoder to select one of sixteen sites per channel. The selected site is connected to the analog data input/output pad through a large CMOS pass-gate to allow externally generated currents to be ‘steered’ to the selected site. A fifth bit, a flag bit, is included with the channel address in order to select between stimulation and recording for the selected site. The flag bit selects either a direct path between the I/O pad and the site or selects the path through a buffer amplifier for recording.

The functionality of the probe is quite simple. A power-on-reset circuit (POR) initializes all of the circuitry to a startup state, which connects all of the sites to the I/O pads to facilitate parallel activation of all of the iridium sites. After activation, the first clock pulse resets the POR circuitry, which then switches the probe circuitry to normal operation. The POR state can also be initiated via a negative strobe on the clock line, CSTB. The strobe sets the POR latch to its ‘power-up’ state, where again it remains until a clock pulse resets it. A strobe on the address line, ASTB, resets all of the addresses to site zero and clears the flags (stimulation mode). Additional circuitry is included with site zero so that while the address line ASTB is held low, site zero is disconnected, thus making it possible to measure the probe leakage current.

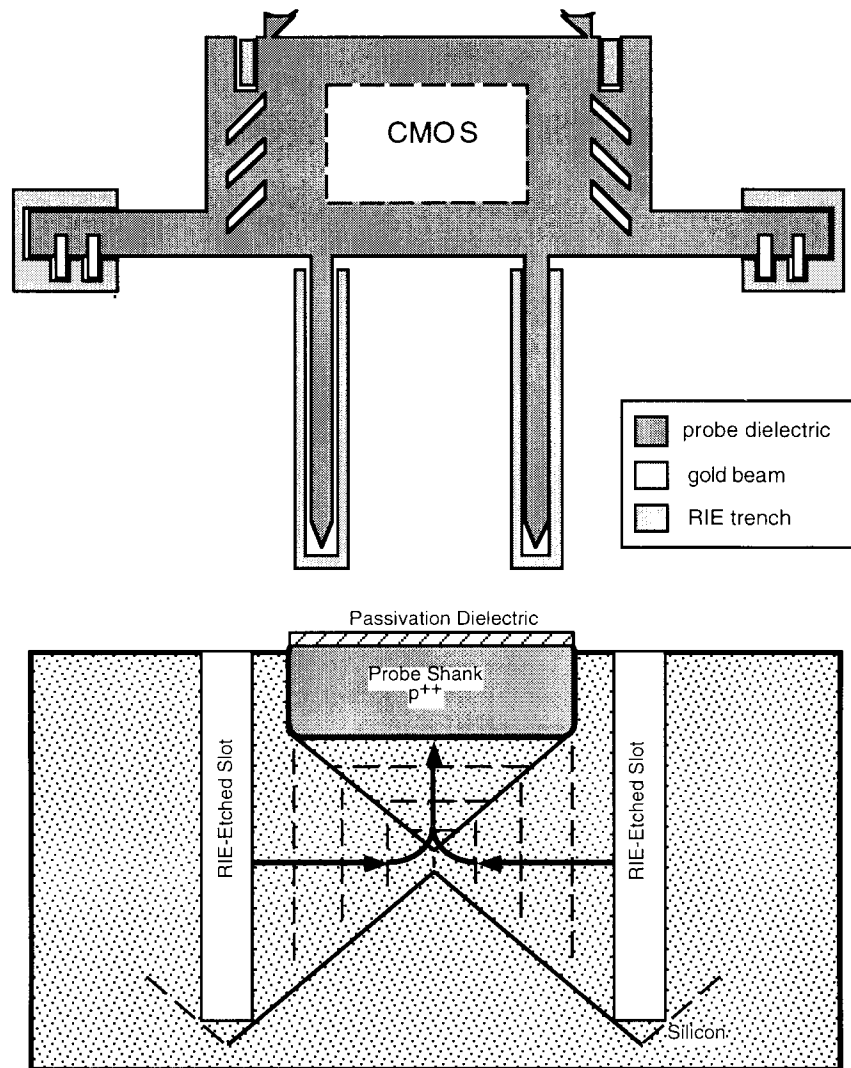


Fig.19: Illustration of the use of deep RIE-etched slots around the shanks and wings of an active probe to speed the release of these areas while preserving thick silicon under the circuit areas. Small corner compensation fillets to prevent lateral undercutting of the circuit areas from the front of the wafer are also shown along the top edge of the probe. The cross-section of a probe shank shown below illustrates how the slot permits lateral etching from the front and early release of the shank.

The STIM-2B probe design was completely simulated, and the results demonstrated that all of the circuitry should work as intended. The layout of the circuit blocks allowed the extraction of circuit parasitics, which were included in the simulation. Because of the mixed tri-level logic nature of the circuitry, all simulations were performed as complete analog simulations at 10MHz. Circuit operation was also verified using different process parameters to be sure that the chip would function normally in the face of process variations. For example, although the target process uses a 400Å gate oxide, correct digital circuit operation was confirmed from 300Å to 500Å, albeit with some speed variations.

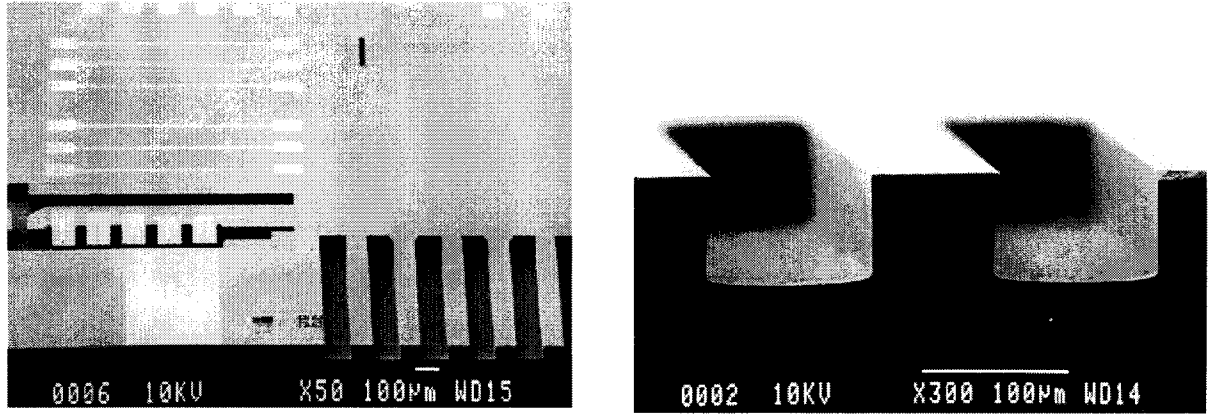


Fig. 20: SEM views of DRIE slots etched in active probe wafers to facilitate early release of the shank and wing areas while retaining thick silicon under the circuit areas at the rear of the probe.

Process technology	Modified bulk micro-machined 3µm n-epi, p-substrate, p-well CMOS process
Power supplies	$V_{CC} = 5V$, $V_{SS} = -5V$, Gnd = 0V
Control signals	Clock, Y-Data, (X-Data)*
Current Range	$\pm 100\mu A$
Current Resolution	External
No. of channels	4
Total chip area	7.1mm ² /probe
Number of site	64 (up to 256)*
No. of sites per shank	4
No. of shanks	16/probe (up to 64 in 4 probe array)*
Shank/Site spacing	400µm
Total external leads	9 (11)* leads (3 power, Y-Data, X-Data* Clock, 4 analog I/O, X-Data Out*)
Time resolution @ 4MHz clock freq.	5µsec (longer if array exceeds 5 probes)*
Site area	1000µm ²
Special features:	<ul style="list-style-type: none"> • per channel recording mode • electrode-activation mode • simple design • mono-multipolar stimulation capability • daisy-chained serial data path design for 3D array extendibility* • programmable 3D array platforms* • enhanced circuit undercut protection • advanced site formation technique

*Stim-3B

Table 1: Specifications for STIM-2B/3B.

QuadraStim-EX

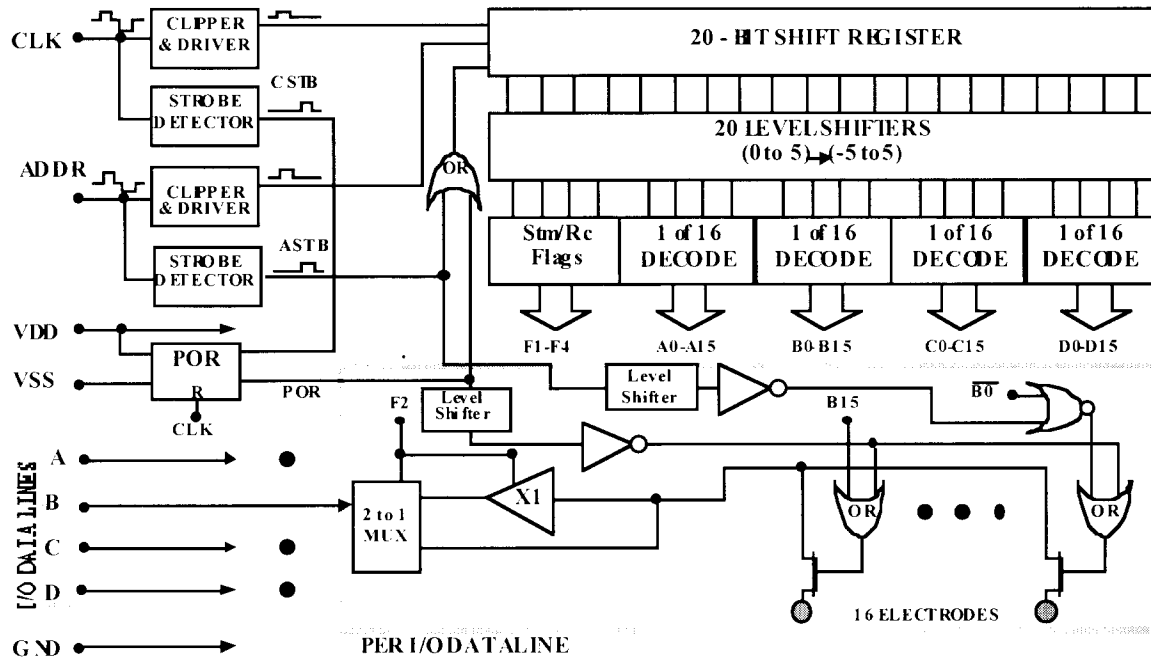


Fig. 21: The functional block diagram of STIM-2B: a four-channel 64-site stimulating probe with external current generation.

In order to realize a version of STIM-2B suitable for use in a 3D platform-mounted array (STIM-3B), it was necessary to add the slots, wings, and beam leads associated with platform use as well as to modify the on-chip circuitry. Several different addressing options were considered for multiple probes in a 3D array. The option chosen is shown in Fig. 22. This arrangement allows the number of overall leads to be kept compatible with our present 12-pin Microtech connectors and is suitable for use with any number of probes. An additional 4b shift register is included on each probe, with each bit being used to select/deselect each of the four I/O lines for that particular probe. The output of the shift register is fed via the platform to the next probe so that an extendable “x-addr” (probe address) register is formed. All of the probes in the array share common analog I/O data lines, power lines, clock lines and y-addr (site address) lines. The same y-addr is clocked into the 20b shift register on all of the probes. While the y-addr is being clocked in, the x-addr is simultaneously being clocked into the first probe and daisy-chained to the second, third, and so forth. In the event of differing register lengths, the shorter register can be padded with zeros. This arrangement requires only ten external leads and allows stimulation on a single probe or across several probes. Almost any combination of four sites across the array can be selected. Since the stimulus currents are externally generated, only four sites can be active at one time unless they are driven in parallel. An additional pull-up transistor was included on the input of the x-addr register on each probe so that the x-addr input lead does not have to be connected when used as a single stand-alone probe. The input will default to logic level 1 and all of the channels will always be active. The platform is designed with air-bridge fuses to provide a direct connection between the successive ‘x-addr in’ and ‘x-addr out’ pads for an unpopulated probe slot; when a particular slot is populated with a probe, the fuse is blown and the data propagates via the on-chip register.

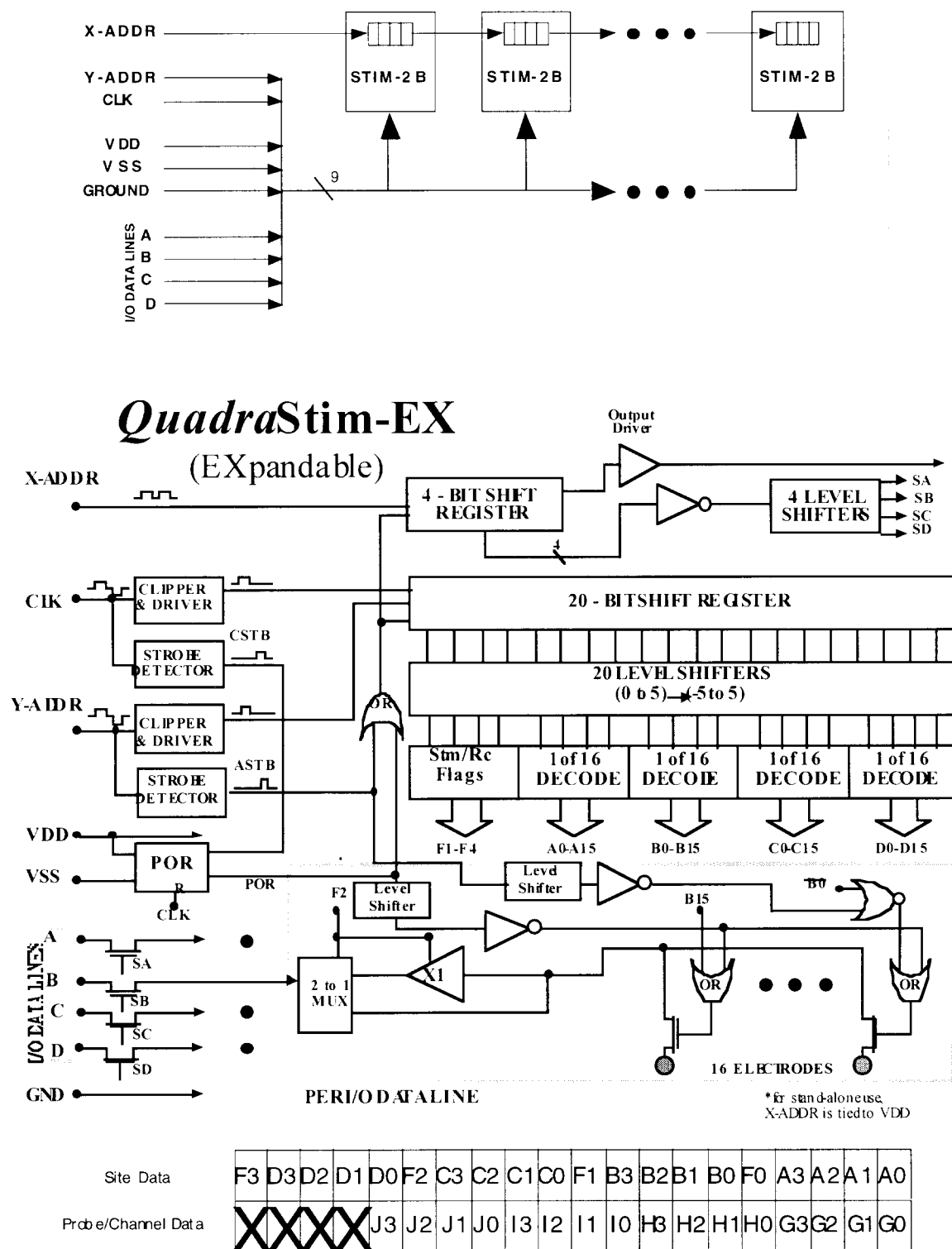


Fig. 22: General architecture and functional block diagram of a multi-probe STIM-3B array. A sample data word for a four-probe (G, H, I, J) array is shown. The sites are designated as A, B, C, and D, with F denoting the stimulate/record flag bits (X=don't care)

The STIM-2B/-3B probes were fabricated using a 16-mask CMOS process. The threshold voltages were -1.08V and $+1.12\text{V}$ for the NMOS and PMOS devices, respectively, with contact resistances of $1\Omega/\text{contact}$ or less except for the contact to p+, which averaged $3.50\Omega/\text{contact}$. The probe circuitry was fully functional with performance close to the design targets. Figure 23 shows the input-output performance of one of the on-chip recording amplifiers. The amplifiers have a bandpass from about 10Hz to 10kHz with a mid-band gain of about 60. This is the same amplifier used on our second-generation recording probe [Ji 92]. It has been shown to have an input noise level equivalent to about $13\mu\text{V-rms}$ over this bandwidth. The functionality of the digital portion of STIM-2B is shown in Fig. 24, where a $100\mu\text{A}$ current is driven into channel A and the output of the selected site is observed across a $1\text{k}\Omega$ load. The circuitry operates at data input rates of up to 4MHz . Figure 25 shows the back side of a STIM-3B probe, illustrating the ability to retain a thick silicon area over the circuit area. Figure 26 shows top views of completed STIM-2B and STIM-3B probes.

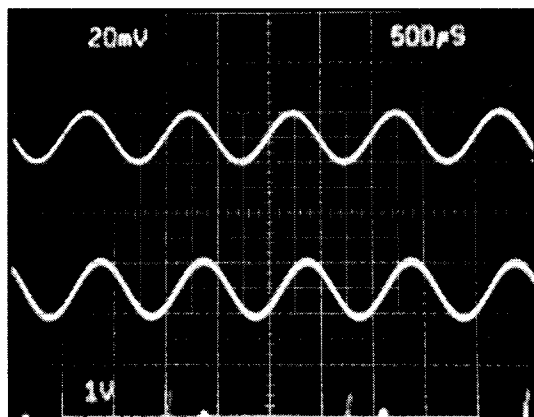


Fig. 23: Scope trace showing a 1kHz 20mVp-p input signal to one of the STIM-2B recording amplifiers (top) and the output signal (1Vp-p) below.

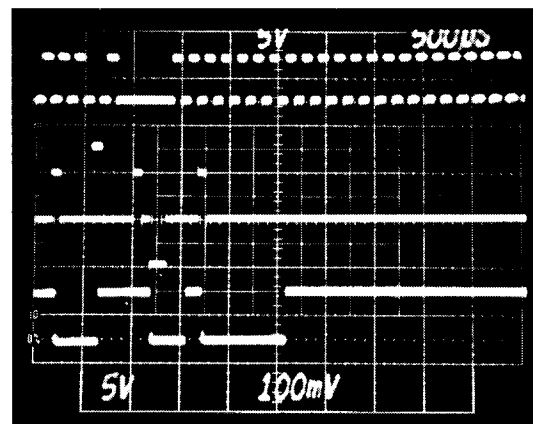


Fig. 24: Scope trace showing clock (top), data, and output of site A0. The POR state, POR reset, and leakage current mode are demonstrated.

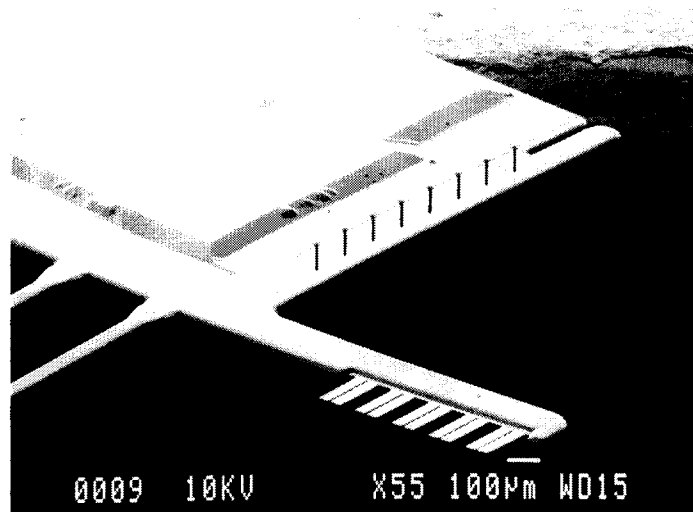


Fig. 25: SEM view showing the back side of STIM-3B. Thick silicon remains over the circuit area even with a 15 minute over-etch beyond probe separation. The jog at upper right was due to an insufficient dielectric corner compensation bridge width and has since been corrected.

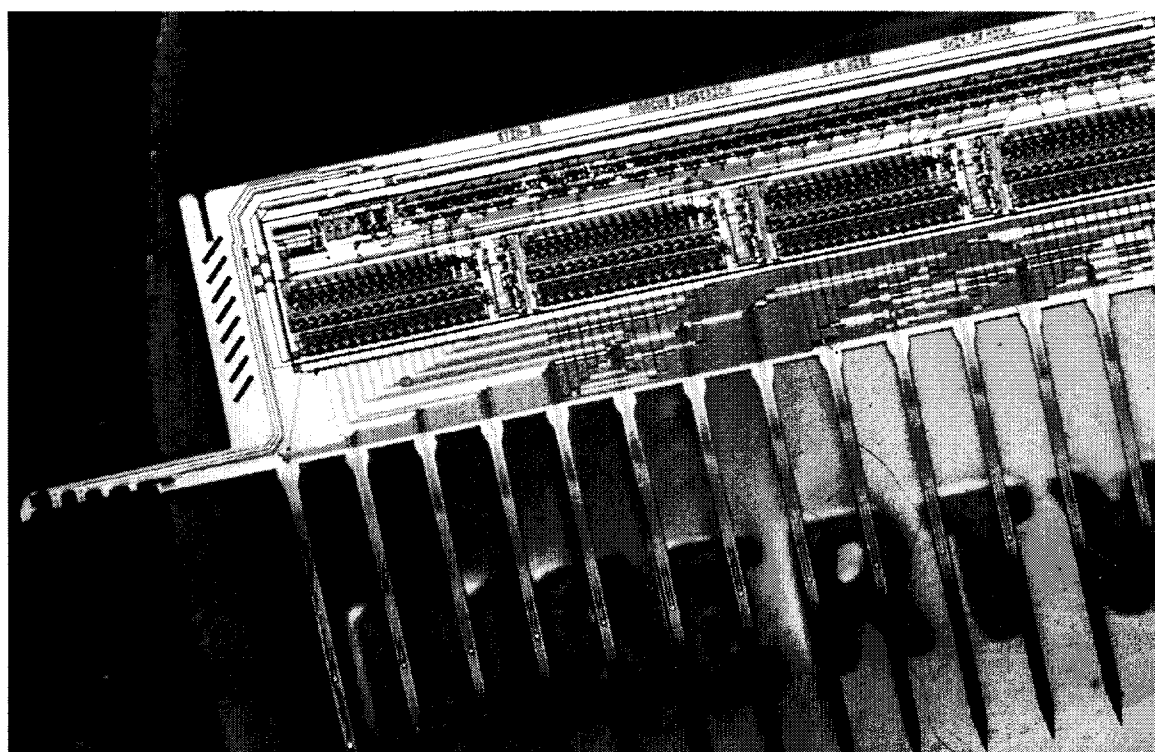
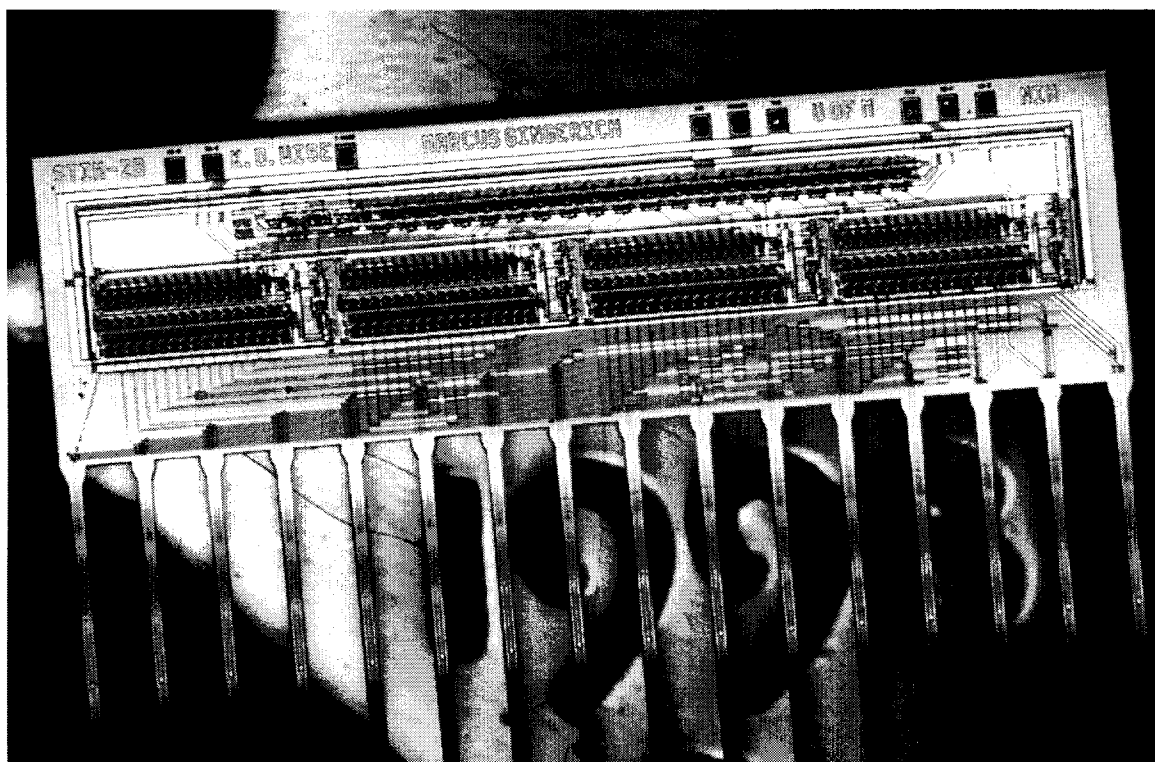


Fig. 26: Photographs of completed STIM-2B and STIM-3B probes. The shanks are on 400 μ m centers with four sites per shank. (*Shown on a Lincoln cent*)

In order to form 3D arrays using STIM-3B, a series of corresponding platforms, cables, and spacers are needed and have been successfully fabricated. As noted above, in order to allow addressing of multiple probes in a 3D array, STIM-3B has an extra 4b serial input shift-register which, when the bits are set, connects the corresponding I/O channel of the probe to a common I/O bus on the platform. All of the extra registers of the probes in a STIM-3B array are connected in series via platform leads to form an extended or virtual register. The virtual register enables all of the probes of a 3D array to be addressed with only two address lines: a channel enable address line and a site address line. This architecture does have a limitation in that it does not allow independent use of the same site address on two separate probes in the array. The slightly reduced flexibility was considered a reasonable sacrifice to achieve a reduction in circuit complexity and, more importantly, lead count. Rather than waste area on the active CMOS probe mask set, the STIM-3B 3D structural pieces were designed on a separate mask set, which required only six masks and was essentially the same fabrication process as is used for passive probes. The only difference is that there are no site or pad masks; instead, there is a single beam/pad electroplating mask. The electroplating mask is used as the final step to form the beam lead interconnects and pads on the platforms after the field etch has been done. The conductor mask was designed with the polarity reversed from what it would normally be for a passive probe so that it could be used in a lift-off process for metal conductors instead of for polysilicon. The first wafers still use polysilicon (patterned by image reversal) and the normal high-temperature dielectrics; future wafers will use low resistance conductors and low-temperature upper dielectrics.

Four different platform designs were included on this mask set, one of which is shown in Fig. 27 just prior to the EDP release etch. This design can be programmed by selectively blowing integrated microfuses with a current pulse. It is the largest platform we have fabricated and can be programmed to hold up to 16 probes. When fully populated, the platform will hold a 16x16 array of four-site shanks, creating a 3D grid of 1024 stimulating sites on 400 μ m centers spanning 1.2mm x 6mm x 6mm (a volume of 43.2mm³). An enlargement of some of the electroplated gold pads and interconnects on a platform and the electroplated gold beam leads on the connector are shown in Fig. 28. One of the microfuses is also indicated in the picture. The microfuse is a bridge of electroplated gold undercut by etching out exposed polysilicon during the EDP release etch. The platforms and the associated spacers and handling discs (which are placed on top of an assembled array for vacuum-pick handling) are shown in Fig. 29 along with one of the STIM-3B active probes. All of the pieces for a 3D active stimulating array are now ready for assembly.

The STIM-2B probe is now in use in acute in-vivo studies aimed at mapping interconnections between the dorsal cochlear nucleus (DCN) and the inferior colliculus (IC) in guinea pig. STIM-2B was placed in the DCN and a multisite recording probe was placed in IC. While recording from the IC, the location of a monopolar stimulation signal (a 97 μ A, 100Hz sine burst, having a duration of 50mSec) was varied electronically in the DCN as shown in the site patterns of Fig. 30. The same stimulus was presented 100 times at each stimulation site in the DCN, while the neural responses were recorded for 100mSec at each site location in the IC and saved for later analysis. This analysis included single-unit spike counts, each spike corresponding to single-cell neuronal discharges. Histograms of the spike counts were used to show the effects of the stimulus on local neural activity. For a fixed recording site in IC, the single-unit spike counts are also shown in Fig. 30 as a function of the stimulus site location. The changing patterns of neural activity are very apparent, with site address B12 primarily responsible for stimulating the connections driving the recorded unit. A high stimulus amplitude of 97 μ A was used for this comparison, but response histograms were observed for stimulus amplitudes as low as 12 μ A at site B12.

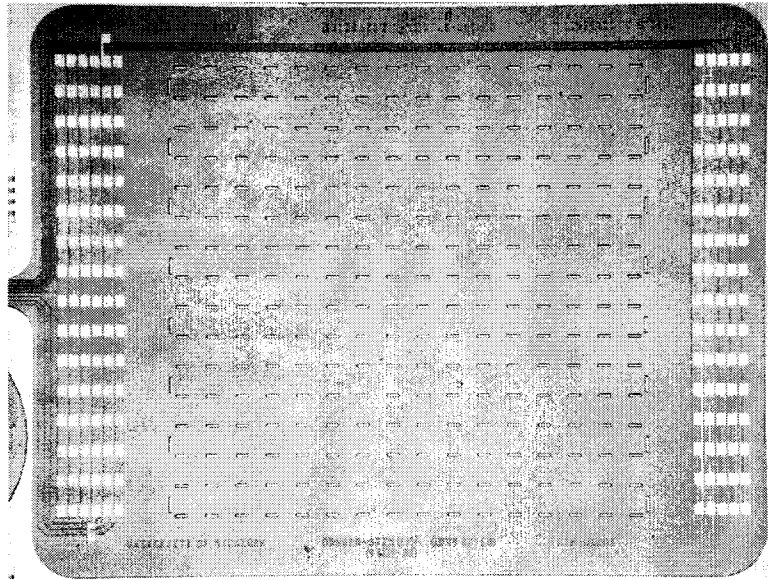


Fig. 27: A photograph of one platform design, which can be programmed via microfuses to hold from one to sixteen probes, creating a 16x16 array of four-site shanks on 400 μ m centers for a total of 1024 stimulating sites.

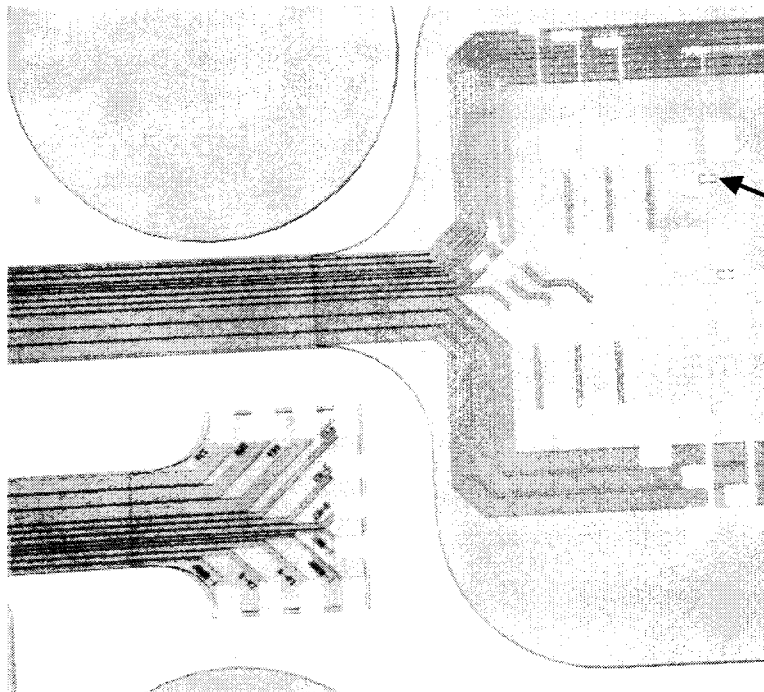


Fig. 28: A close-up of some of the electroplated gold interconnects and pads on a platform and the beam leads on the connector end of a ribbon cable. The position of one of the platform's microfuses is also shown.

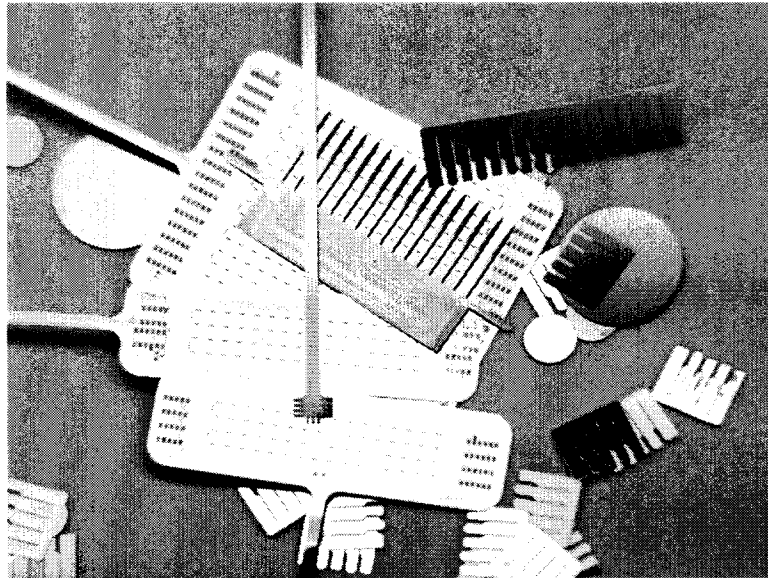


Fig. 29: A photograph of several of etched-out platform designs, spacers, and a STIM-3B probe.

In separate *in-vivo* experiments, the recording ability of the probe was evaluated. Recording with the on-chip amplifiers was sometimes difficult because of DC baseline drift, which occurs due to electrochemical instabilities at the iridium electrode-electrolyte interface and optically-generated currents at the input to the amplifier. The amplifiers were designed to reject DC shifts of as much as 100mV, but some apparent shifts in the DC baseline can be as high as several hundred mV, which drives the amplifiers into saturation. High-resistance (100M Ω) input clamps are being added to the amplifier inputs to eliminate these problems. The possibility of using the probe as a simple site selector, connecting the sites directly to external amplifiers, was also evaluated with satisfactory results, demonstrating a high signal-to-noise ratio even without on-chip amplification. While the lack of on-chip amplification reduces recording performance, especially for more distant or lower-amplitude single units, the demonstrated ability to record without amplification makes this probe a very powerful tool in studying the CNS. For example, by using two of the new probes and automatically scanning both the stimulus and the recording patterns, the organization of the pathways between the DCN and IC could be mapped rapidly. Such mapping would be virtually impossible using discrete wire electrodes.

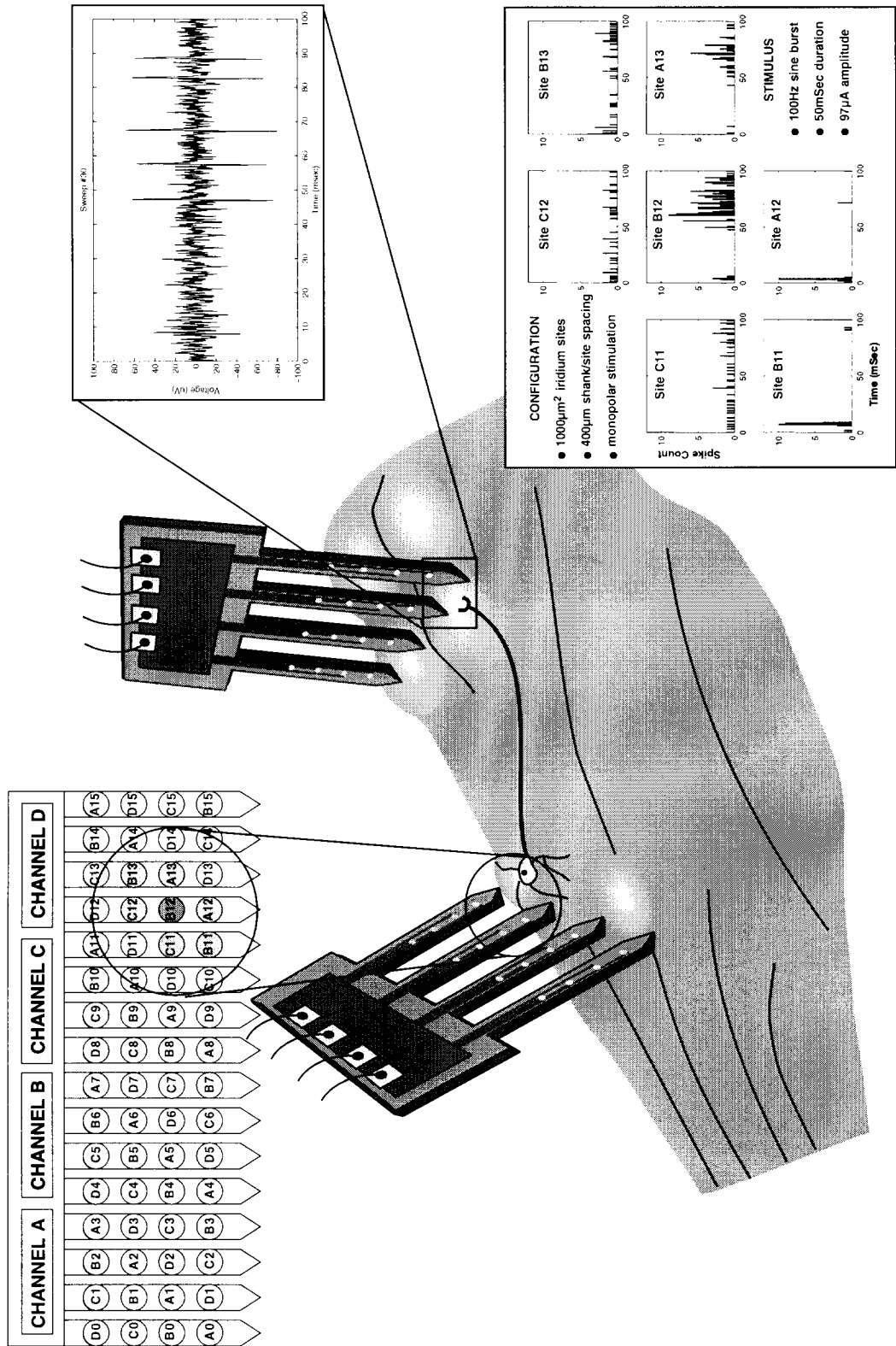


Fig. 30: DCN-IC Mapping Studies. The site locations for a stimulating probe inserted in DCN are shown along with the histograms from a single unit in IC are shown in response to those stimulus sites. Mapping can be done automatically without moving either probe.

5. STIM-2: A 64-Site 8-Channel Active Stimulating Probe with On-Chip Current Generation

The high-end probe in this family of stimulating probes is STIM-2, a 64-site 8-channel device with on-chip current generation. This probe will be the basis for a 1024-site 128-channel 16-probe stimulating array capable of testing the feasibility of a visual prosthesis in a meaningful way.

This probe features more extensive on-chip circuitry and, in a future 3D version as STIM-3, will be extendable to multi-probe 3D assemblies. The electronic system designed for this probe allows the selection of any of 64 sites in both normal and special modes for either stimulation or recording. This selection scheme is globally multi-polar since the time delay of 4 μ sec to select the next site is negligible at the clock frequency of 4.5MHz, appearing effectively simultaneous to the tissue. The probe allows stimulation through eight sites simultaneously, and any one of these sites can be monitored (recorded from) at any time. Table 2 gives a brief summary of the specifications and special features for this second-generation stimulating probe.

Table 2: Specifications of STIM-2

Process technology	3 μ m, p-substrate, n-epi, p-well single poly, double metal two-step diffusion micromachined CMOS technology
Supply voltage	V _{cc} = 5.0V, V _{ss} = -5.0V, GND = 0V
Control signals	DATA and CLOCK
Current range	-127 to +127 μ A
Current resolution	1 μ A
Power dissipation	Standby \leq 50 μ W, Operating \leq 10mW
Clock frequency	4.5 MHz (~222 nsec)
Time delay to select any site	4 μ sec
Total external pads	5 pads (VDD, GND, VSS, DATA, and CLOCK)
Electrode site size	1000 μ m ² (optional for 400 μ m ²)
Probe shanks	8 and 16
Total stimulating sites	64
Chip area with boundary	11.2 mm ²
Circuit features	<ul style="list-style-type: none"> • low-impedance shunt mode for idle sites • anodic-bias mode for high current delivery • electrode-impedance monitoring mode • electrode recording mode • self-test and trouble flag modes • electrode-activation mode • simple level-shifter, no static power dissipation • clock-controlled address decoder • low power current source (DAC)

The STIM-2 system is configured as shown in Fig. 31. Each group of eight electrodes, placed on one or two micromachined silicon probe shanks, is connected to a front-end site selector (an 8-to-1 multiplexing array) and is controlled by a DAC. Up to one site from each group can be selected for stimulation. As special options, several different modes are implemented, including a site-activation mode, a site-impedance test mode, a neural recording mode, a low-impedance shunt mode for unselected sites, a

Table 3: The various operating modes of STIM-2

<i>Mode</i>	<i>Operation</i>
Normal Stimulation	DAC drives the selected site through the site-selection transfer gate
Site Activation	Occurs on power up; all sites are connected to the data line to be activated by cyclic voltammetry
Impedance Test	The voltage of the selected site is transmitted off-chip on the data lead so that it can be monitored during current stimulation, permitting the site impedance to be assessed.
Recording	The selected site is monitored through a recording amplifier so that neural activity can be observed.
Low-Impedance Shunt	Outputs of inactive channels are connected to ground to remove any potential that might build up on the site due to charge imbalances.
Anodic Bias	The sites are connected to a bias of about 0.6V instead of to ground to equalize the charge that can be delivered from the probe in cathodic first operation.
Trouble Flag	Causes the probe to pull down the data line if a series of monitoring points on the chip are operating normally.
Current Calibrate	Allows current stimulation but shunts that current to the ground return line so that the current at a particular setting can be externally monitored and calibrated.
Platform Address	The incoming address is treated as a probe address, allowing subsequent data entry to be steered to a different probe by circuitry on the platform. This address causes no operation on the present probe itself but only causes action in the platform circuitry.

Thus, STIM-2 has a variety of modes to allow its performance and operating characteristics to be fitted to a given application. The current design was fabricated during this contract and desired design changes have been identified. Future design modifications include the possibilities of making anodic bias the normal situation, allowing multiple interpulse bias levels, adding separate output line(s) for recording, or adding a per-channel time-out feature (as on STIM-1). Since setting the interpulse bias level is global for all sites, it is a simple matter to issue a command to turn this option on or off. An on-chip DAC would allow this level to be set as desired and would allow important experiments on the influence of bias not only on safe charge delivery but also on tissue encapsulation of the sites. So long as the time-out feature does not excessively compromise the die area, it is a useful safety feature, even though additional software safety checks are also used. It should be noted that, as on STIM-1, a self-test (trouble-flag) mode is still built into every frame and it is at the discretion of the external electronics whether to wait for the data line to fall ("I'm OK!") and look at this signal. This flag causes the probe to pull down the data line during the test period of the frame interval unless a problem (such as time-out) is detected by the on-chip circuitry.

Data Designations

A detailed view of the timing and bit designations in STIM-2 is given in Figs. 32 and 33. The upper diagram illustrates the situation when normal data are transmitted to the probe as a 16-bit word instruction. A 16-bit word is serially clocked into the 8-bit serial shift register from the data line. The first two bits represent the desired mode, followed by six address bits. The first three address bits are decoded to select one of the eight DACs, and the second three bits are decoded to select one of eight sites associated with that DAC for stimulation. During half of the ninth time slot, the data line goes low to negative voltage, causing the mode and address latches to latch those bits. Eight bits of current data are then clocked in. These eight bits, representing the amplitude and sign of the sinking or sourcing currents, are directed into the selected level shifters. A strobe then occurs on the clock line, latching these data, followed by a high impedance state that occurs during the last bit time, allowing the probe to transmit the "I'm OK" signal back to the external electronics by pulling down the data line. The remaining three possible combinations of modes are for recording (M01), low impedance shunt (M10), and extended data word (special mode) (M11) operation.

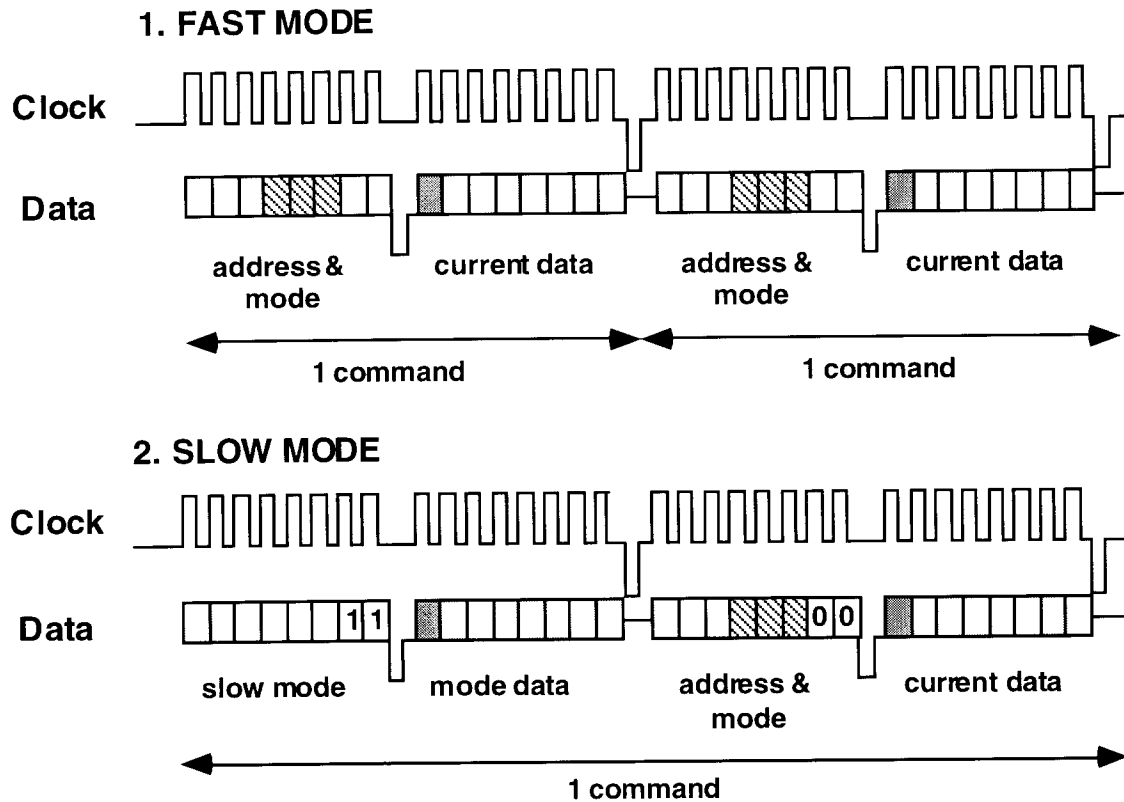


Fig. 32: Overall timing diagram for STIM-2 operation.

The lower portions of Figs. 32 and 33 illustrate the use of a 32-bit instruction for cases which do not require high-speed operation. Once again, the first and second parts of the address and the mode bits are clocked in and latched on the data strobe. At this time, the mode bits are "11", indicating an extended instruction for special modes. In this case, the first three address bits in this first word are interpreted as special mode information and

are latched to allow up to eight special modes. For example, at present the first four special modes are designated for anodic bias, impedance test, current calibration, and platform address as noted in Fig. 33. These could be used to address as many as 256 ($=2^8$) different probes in a distributed system, each probe having 64 sites. One special mode could be defined to allow a third data word as well, allowing the address space to be expanded further. The second 16-bit data frame is a standard probe command as used in a single instruction.

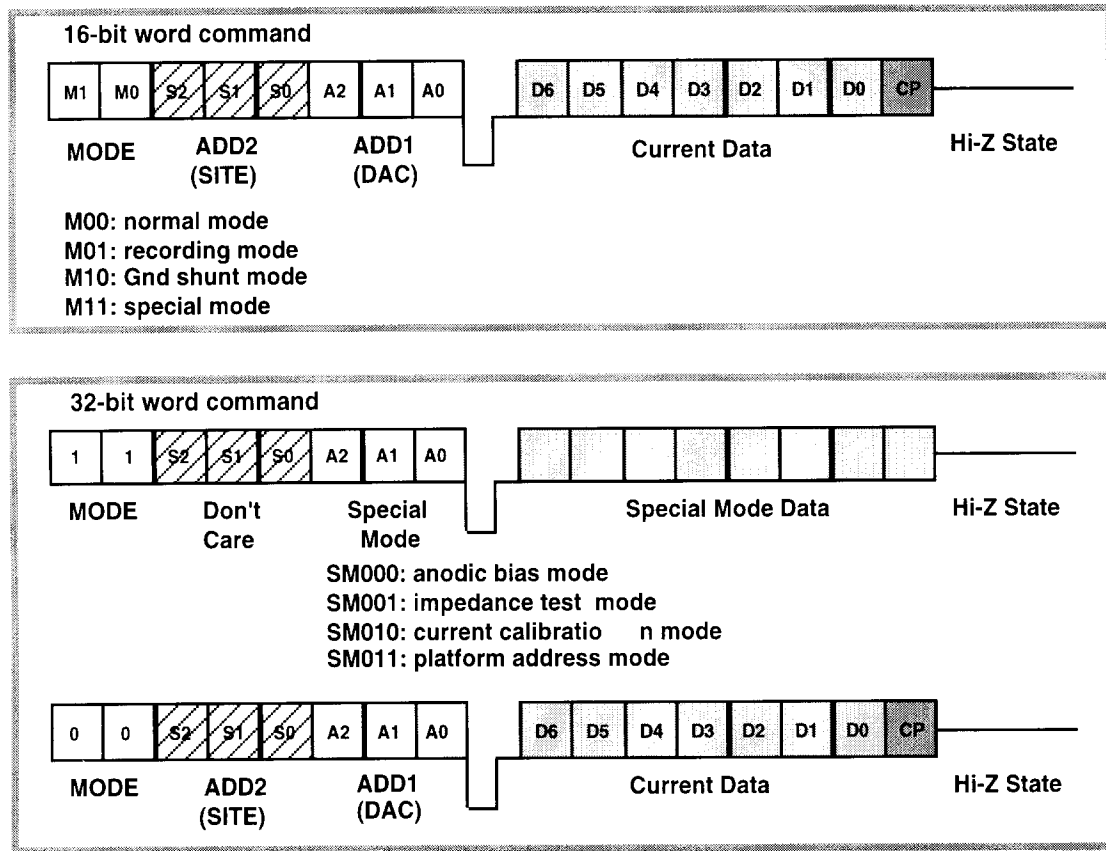


Fig. 33: Data designations for the second-generation stimulating probe.

Channel Selection and Stimulation Patterns

There are many useful combinations of stimulation patterns that could be used with 64 sites. In order to allow a wide selection of these and yet maintain a reasonable level of complexity in the selection circuitry, a simple two-shank combination scheme has been chosen for STIM-2. Figure 34 shows a few of the possible stimulation patterns that can be implemented using this simple two-shank combination option. Each DAC can be switched to any one of eight sites, distributed over two adjacent shanks. In this example, DAC1 controls sites 1-8, while DAC2 controls sites 9-16. This allows any two adjacent sites to be selected, for example, either laterally or in depth. A wide variety of patterns are possible. Figure 35 shows the physical probe shapes and site address maps for the 8-shank and 16-shank versions of STIM-2, respectively. Using this scheme, any two adjacent sites can be addressed and used for bipolar stimulation.

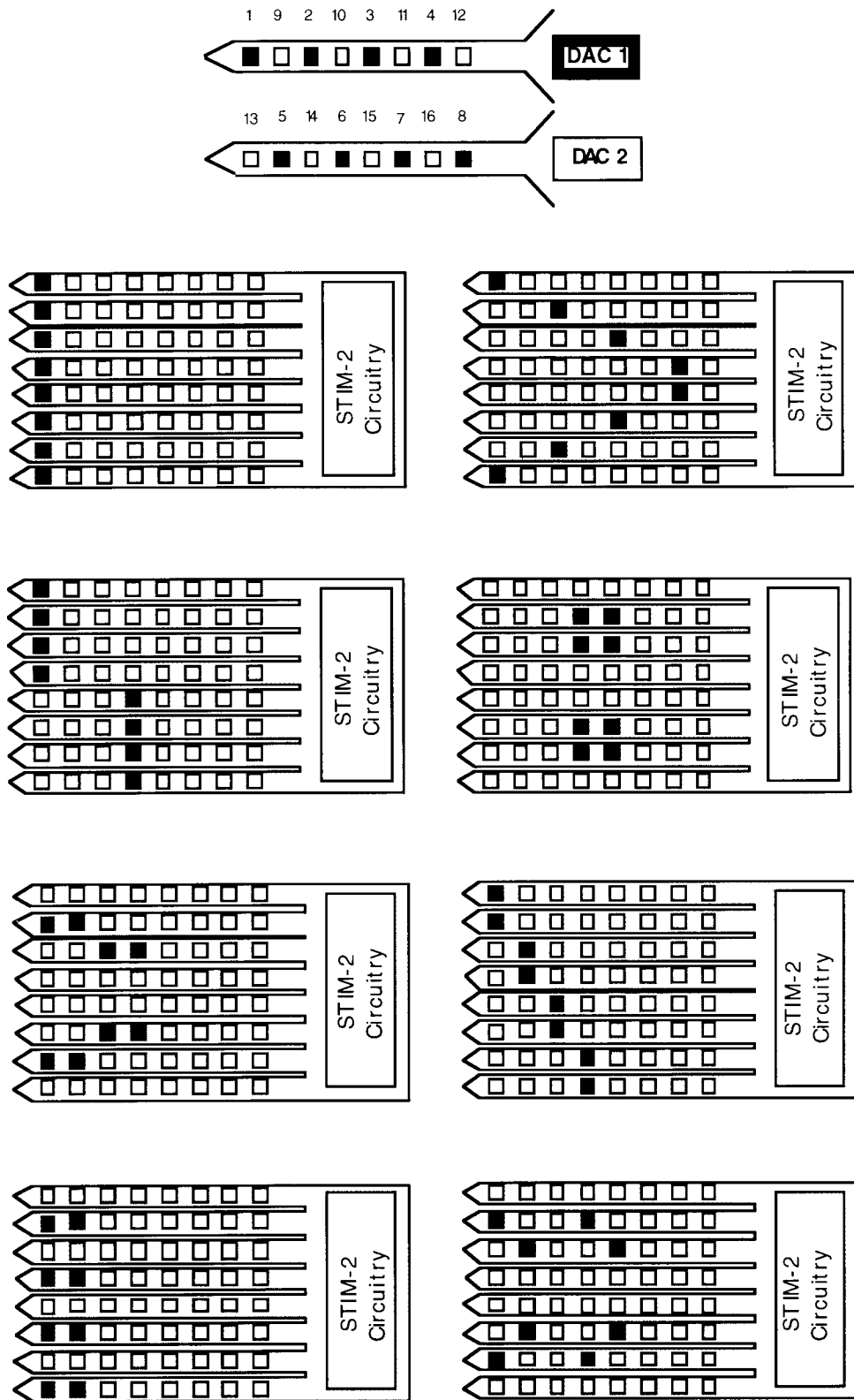


Fig. 34: Examples of possible stimulation patterns using a simple two-shank combination option for the organization of the DACs and the site selection matrix.

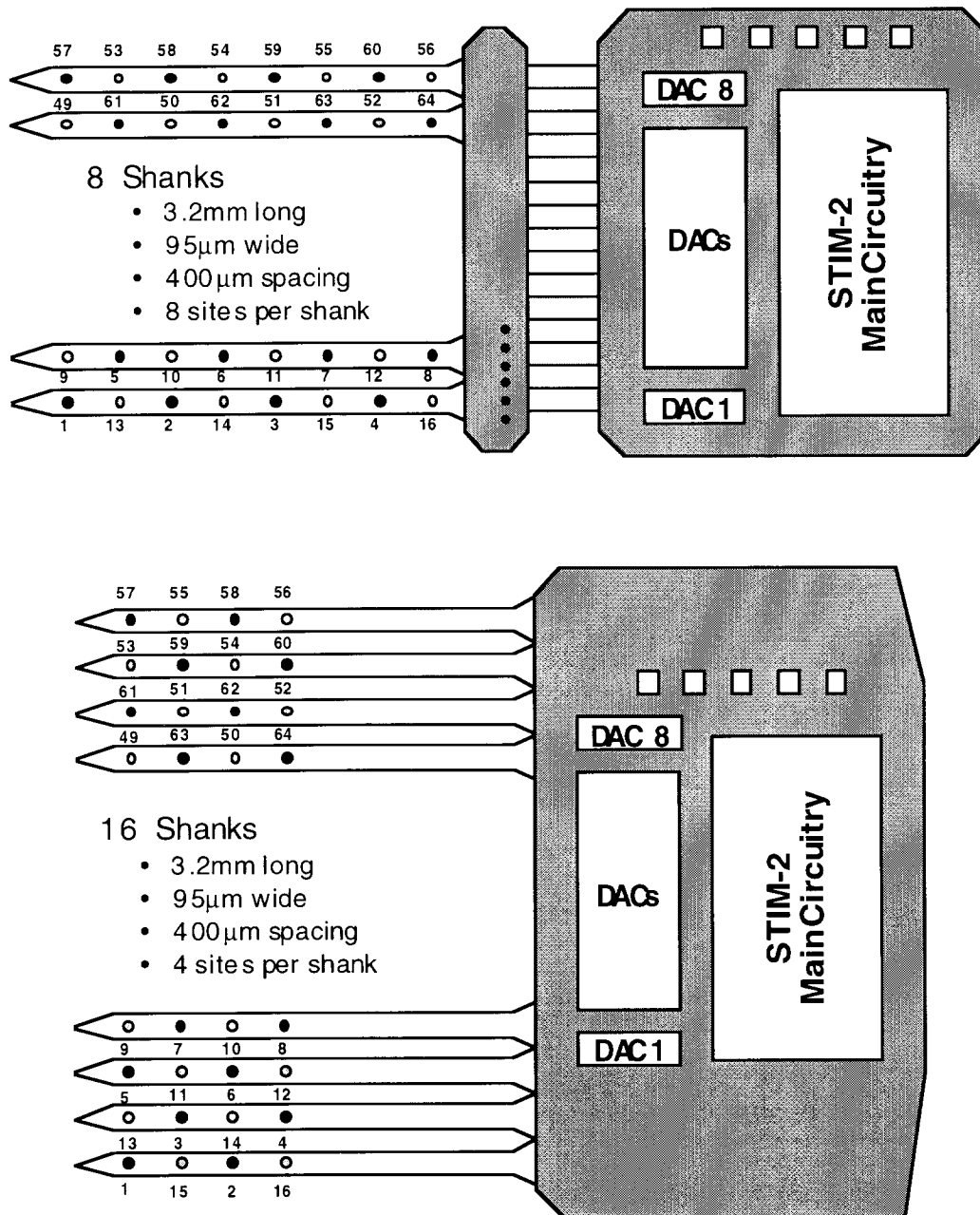


Fig. 35: Physical shapes and site maps of STIM-2. (a) 8-shank version (above) and (b) 16-shank version (below).

Probe Height Optimization

For the actual in-vivo application of these stimulating probes, their height above the cortex, which is determined by the circuit dimensions implemented in the probe, must be low enough to allow the dura to be folded back over the implant so that tissue overgrowth does not anchor the implant area to the skull. While the maximum allowable probe profile above cortex is not known at this time, it is assumed that this rise should be less than 1mm.

However, as additional useful features are implemented on the probes, the chip size naturally increases, making a low profile increasingly difficult. In iterating the design of STIM-2, we will attempt to minimize the height of the circuit area by using the full width of the array. On a 16-shank probe, this is 6.4mm. However, it is also possible to fold the circuit portion of the probe so that it lies flat against the cortex. The idea is that flexible bending bridges (implemented with the shallow boron diffusion used for the probe tips and cables) can be inserted between probe shanks and circuitry so that the circuit areas can be bent over against the circuitry. The perspective view of such a probe is shown in Fig. 36. One of the versions of STIM-2 has been designed with this approach. Photographs of completed STIM-2 probes are shown in Fig. 37.

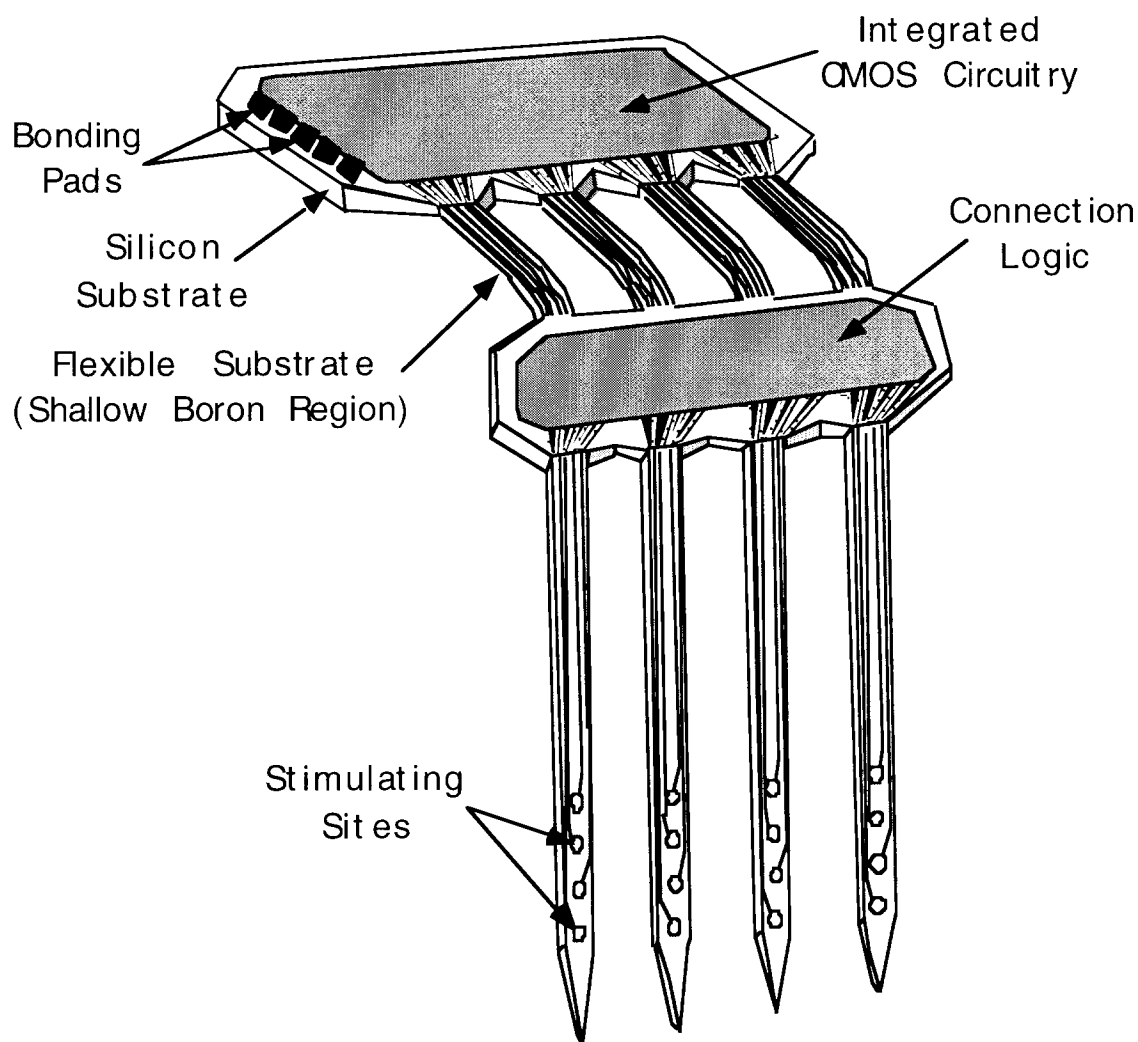


Fig. 36: Perspective view of one version of STIM-2 in which flexible ribbon cables are between the probe body and the circuitry, allowing a low-profile above the cortex for the chronically-implanted structure. For a true 3D assembly, wings would be added to the logic containing the connection logic to allow platform mounting.

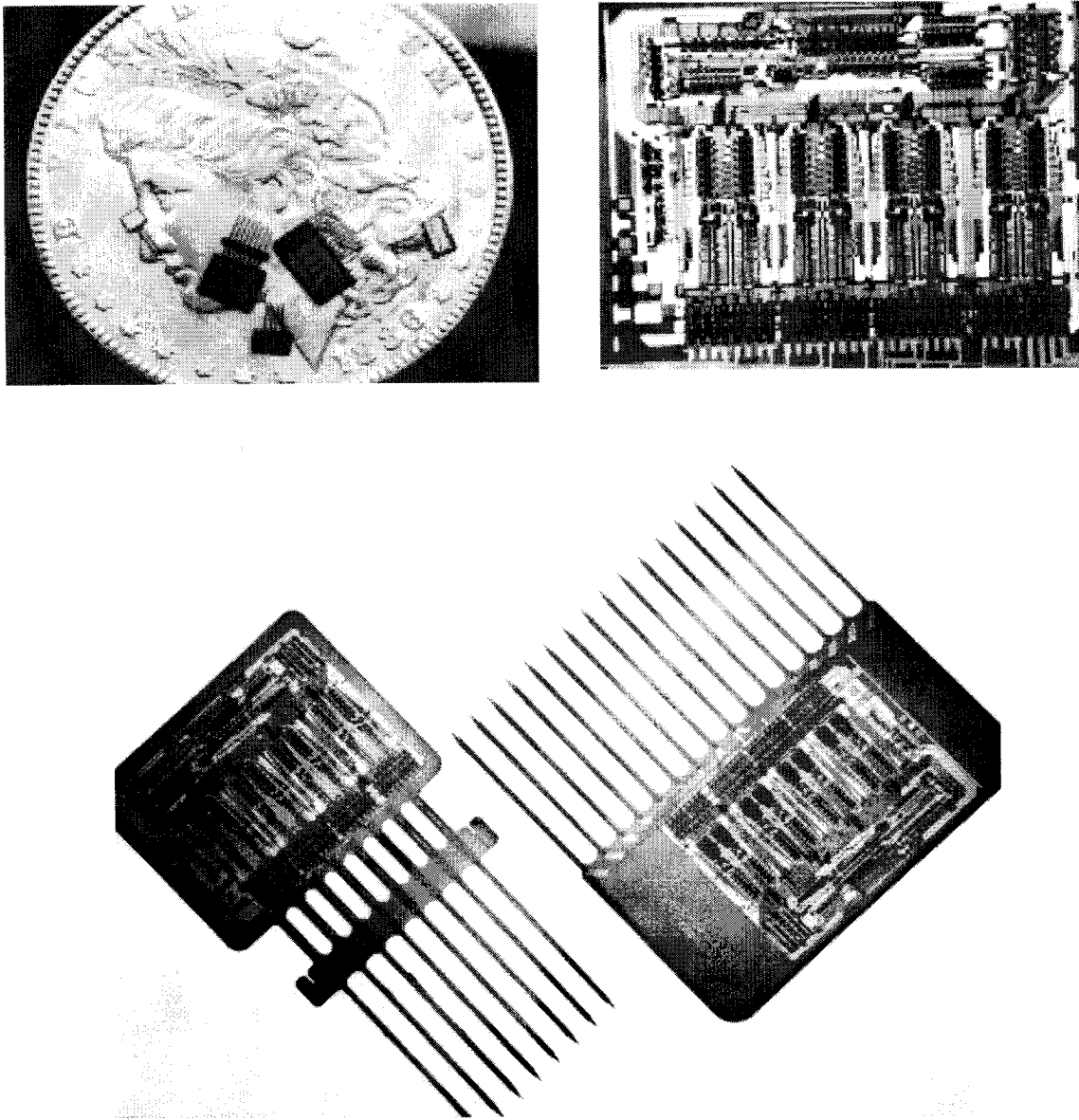


Fig. 37: Above: The various active stimulating probes on a silver dollar: Left to right: STIM-1b, STIM-2; STIM-1a; STIM-2; and STIM-1. An enlargement of the STIM-2 circuitry is shown at right. Below: The two versions of STIM-2.

STIM-2 was fabricated using a 12-mask version of the micromachined CMOS process described above. The most recent fabrication run was prior to the process improvements that eliminated hillocking, improved the contacts, and ensured the early release of the shanks to allow thicker silicon to be retained under the circuit areas of the probe. As a result, the yield of STIM-2 probes that were fully functional was low enough to preclude their use in in-vivo experiments. In addition, in-vitro characterization identified circuit problems where improvements were needed. Accordingly, after thoroughly testing STIM-2 in-vitro, we went back and solved the remaining process problems, using STIM-2B as a process vehicle. We are beginning to perform a final iteration on STIM-2, adding a 3D platform-compatible version (STIM-3) as we did with the development of STIM-3B.

In the last fabrication run of STIM-2, there were three process problems encountered, involving poor contact resistances, aluminum hillocking (which caused breaks in the LTO and attack of the aluminum interconnect in the EDP release etch), and insufficient bulk silicon retention under the circuit areas. The high contact resistances were eliminated using thick (500Å) titanium plugs in the contacts. This prevents aluminum migration into the silicon during the thick LTO deposition. Hillocking is prevented by using stacked layers of titanium and aluminum for the metallization instead of aluminum alone. Finally, the circuit area protection problem was solved using dielectric corner compensation together with deep RIE trench etching from the front of the wafer. The DRIE step ensures lateral undercutting of the shanks so that the process window for retaining thick silicon under the circuitry is substantially enlarged. It should be noted that this problem was especially difficult for the version of STIM-2 that has short ribbon cables between the shanks and the circuitry, allowing the circuitry to lay flat against the cortex. Since these cables are typically in line with the probe shanks and hence aligned with the $\langle 110 \rangle$ crystallographic directions in silicon, they do not undercut at all from the front of the wafer. Hence to allow the back etch to thin them to the 2-3µm associated with the ribbons would eliminate all of the substrate from under the circuitry. This same problem appeared to preclude the formation of ribbon cables on active probes. Rotating the probes with respect to the crystallographic axes of the silicon was tried, and it improved the undercutting of the cables from the front, but at the expense of worse corner undercutting. The use of deep RIE trenches from the front solves this problem by allowing the ribbons to be undercut laterally. Hence, all of the processing problems associated with STIM-2 have been eliminated. It can also be noted that all of the associated processes are available commercially as well. We recently purchased an STS deep RIE tool for our laboratory so that this technology is now available in-house.

Some of the fabricated STIM-2 probes were fully functional in spite of the above problems, allowing complete in-vitro testing to be performed. In most respects, the probe performance was very close to the design targets as shown in Table 4 below. Although the p-channel threshold voltage was low, the functionality and speed of the probe were little affected. The on-chip amplifier, similar to that on STIM-2B and reported earlier [Ji 92] was also fully functional. One architectural change that appears desirable on this probe is to add a dedicated output line for the recording channel. In the present design, any selected site can be connected to this amplifier but the output is over the input data line, which must be floated externally and becomes bidirectional. As soon as clock is applied, however, the amplifier is released and the line becomes a normal data input line again. Thus, recording can only take place for a very short duration (the length of the current pulse(s) being applied). This is not long enough to be very useful if looking at spike activity although it is useful for examining stimulus artifact.

Figure 38 shows the DAC circuit used on STIM-2. Positive and negative reference currents are established in the left-most circuits shown and are used to bias the gate rails of the sourcing and sinking transistors, which are ratioed over a range of 64:1. The outputs of these two transistor banks are gated through series switches controlled by the input current amplitude data, summed, and fed to the selected sites. Figure 39 shows the output of an isolated DAC circuit as it is stepped through its entire range $\pm 127\mu\text{A}$ into a 7KΩ load. Figures 40 and 41 show two views of probe operation, displaying the output voltage waveforms across a 20kΩ resistor load for 8 current levels over its full $\pm 127\mu\text{A}$ range and for 16 levels in the sourcing mode, respectively.

The primary electrical problem encountered when testing STIM-2 was associated with the very slow turn-on of the sink current on many of the fabricated devices. Indeed, looking at the transistor ratios in the DAC circuit of Fig. 38, the reference currents are set much lower than needed and, especially when thresholds miss their targets, can be less

than $1\mu\text{A}$. Since they are established by two different transistor strings, it is difficult to match the sourcing and sinking currents or to accurately set their levels. Hence, it is necessary to calibrate each probe and trim the supply voltages in order to obtain appropriate charge balancing. Furthermore, when the control block is switched on, these currents must charge the long gate rails of the ratioed sourcing and sinking transistors. With the gate capacitance from 127 transistors on each rail, this is a very slow process if the reference current are too low. Indeed, this was true on many of the probes, and as Fig. 42 shows, the negative pull-down can sometimes take more than $60\mu\text{sec}$. The simulation also shown in Fig. 42 shows this behavior clearly, and simulations at other nodes have established that it is indeed due to the slow response of the sinking gate rail.

Table 4: Performance summary for STIM-2 at $\pm 5\text{V}$ compared with the simulated design targets.

Items	Designed	Measured
V_{TN}	0.7 V	0.628 V
V_{TP}	-0.7 V	-1.03 V
$KP_{\text{max}} (= \mu_n \cdot C_{\text{OX}})$	$70 \mu\text{A}/\text{V}^2$	$73.5 \mu\text{A}/\text{V}^2$
$KP_{\text{max}} (= \mu_p \cdot C_{\text{OX}})$	$55 \mu\text{A}/\text{V}^2$	$43.0 \mu\text{A}/\text{V}^2$
DAC linearity	1.0	0.98
• V_{cc} sensitivity	–	7.3 %/100mV
• V_{ss} sensitivity	–	5.6 %/100mV
Standby current	$\leq 10 \mu\text{A}$	$\sim 12 \mu\text{A}$
Maximum of V_{cc}	–	$\sim 9.3 \text{ V}$
Level shifter	$\geq 5 \text{ MHz}$	5.7 MHz
Shift register	$\geq 5 \text{ MHz}$	5 MHz
DAC	$\geq 5 \text{ MHz}$	$> 10 \text{ MHz}$
Address decoder	$\geq 5 \text{ MHz}$	$> 10 \text{ MHz}$
Negative pulse detector	$\geq 5 \text{ MHz}$	$> 10 \text{ MHz}$
$V_{\text{CC,turn-on}}$ (POR)	0.7 V	0.75 V
Op amplifier gain	32.3 dB	29.5 dB
• 3-dB bandwidth	60 Hz-12.6 kHz	50 Hz-9.0 kHz
STIM-2 operation	4.5 MHz	$\sim 5 \text{ MHz}$

In order to allow more accurate charge balancing and eliminate this slow pull-down, we have explored a number of other DAC designs. A promising approach that overcomes these problems is shown in Fig. 43. Here, the reference current has been increased in magnitude and is not switched (it is on all the time). Secondary reference currents are also eliminated, reducing the power dissipation and layout area. This DAC or a similar circuit will be used on the new version STIM-2 now being developed.

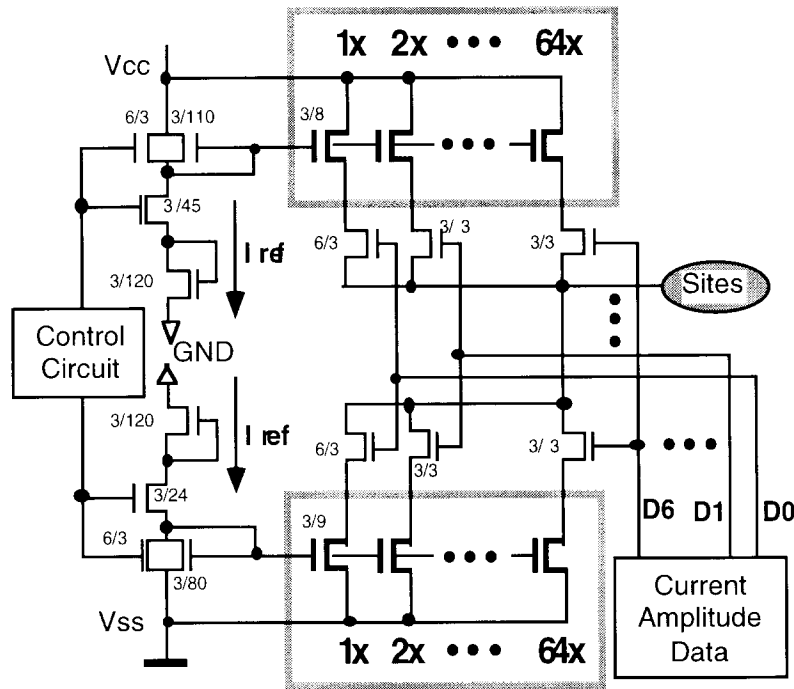


Fig. 38: Overall circuit schematic of the low-power current-output DAC.

More details on these probes can be found in the quarterly reports, in the cited papers, and in the doctoral dissertations of Steven J. Tanghe [Tanghe 92-2], Changhyun Kim [Kim 94-2], and (soon) Marcus Gingerich.

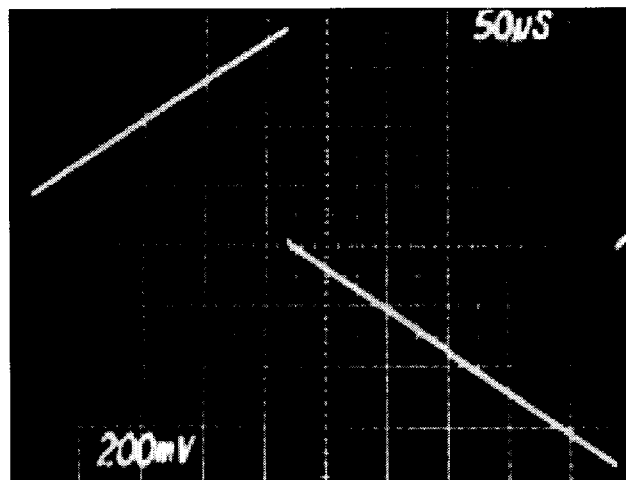


Fig. 39: Test results from one DAC of STIM-2 as the input is stepped through all possible outputs from 0 to +127 μ A and then from 0 to -127 μ A into a 7K Ω load. Current linearity is better than 98%. The circuit operates to frequencies above 10MHz.

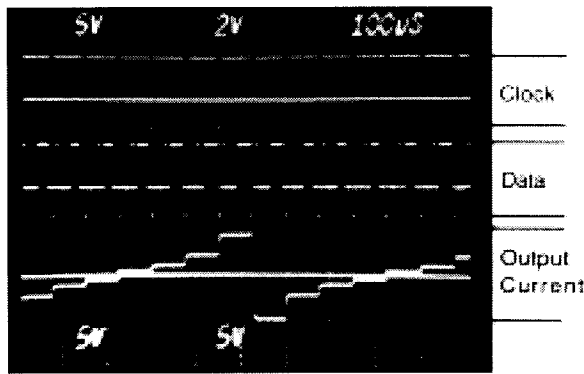


Fig. 40: Probe output as the input data is cycled through its full range (0 to $\pm 127\mu\text{A}$ across a $20\text{k}\Omega$ load using only the most significant four bits, one at a time, giving four states per polarity.

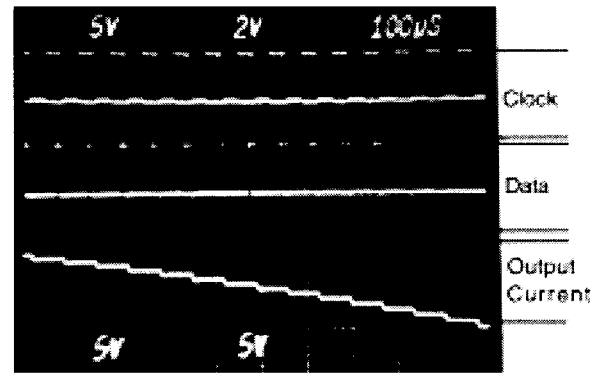


Fig. 41: Probe output across $20\text{k}\Omega$ as it is stepped down through 16 levels using the 4 MSBs of the current level word ($+127\mu\text{A}$ to $+7\mu\text{A}$ in $8\mu\text{A}$ steps)

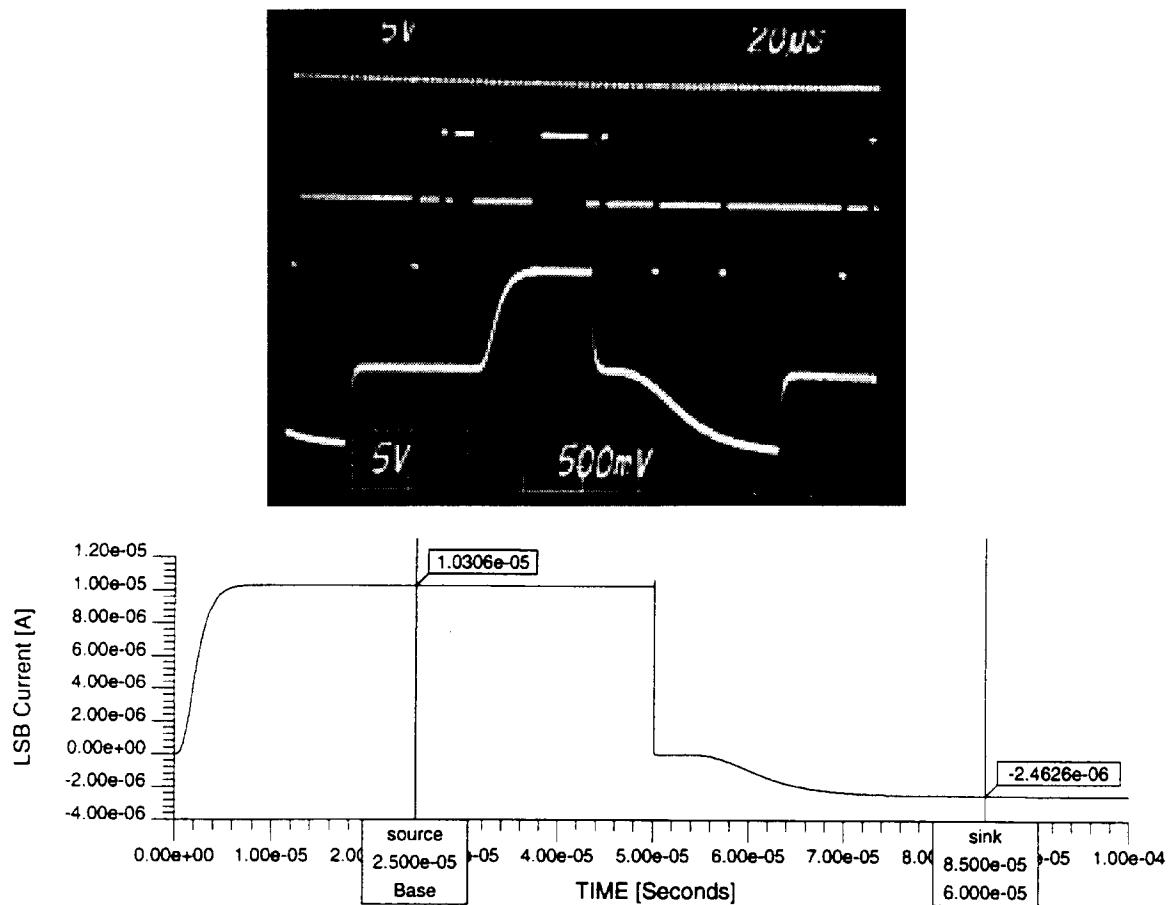


Fig. 42: The output of STIM-2, which demonstrates the slow turn-on of the DAC current sink even with the negative supply voltage turned up to increase the sink current.

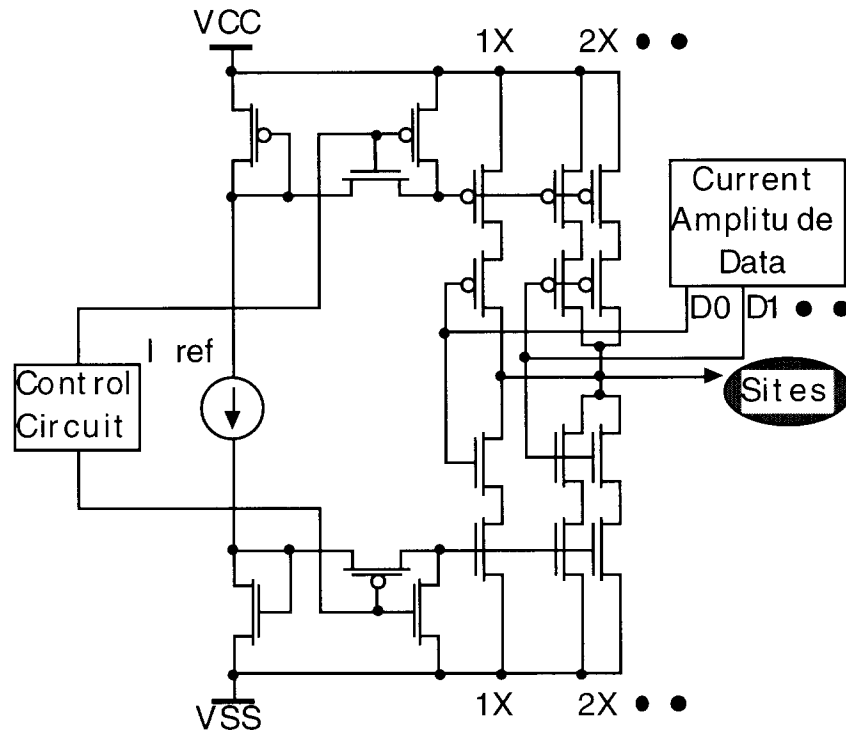


Fig. 43: Schematic of an improved STIM-2 DAC design, which uses a switch in the mirror path to realize on/off control of the sourcing/sinking sections of the DAC.

STIM-3 Test Structures

In order to prepare for the design and fabrication of the STIM-3 system, several test probe structures were included on the STIM-3B 3D platform mask set. These structures were intended to test the feasibility of folded-down circuitry on this probe for reduced height in a 3D probe array. The structures were also intended to test how well the circuit area could be protected from undercut using properly designed dielectric bridges. Figure 44 shows one of the test probe structures. Dielectric bridges are included at the corners of the back-end circuit area in order to protect them from undercut. Multiple dielectric bridges are also included between the flexible interconnects in order to provide protection for the front edge of the circuitry, which in the past has been susceptible to undercut due to the early breakthrough of the backside etch plane in the wider areas between the shanks or in this case the flexible interconnects. Four different test structures were included: one with long straight flexible interconnects, one with short straight flexible interconnects, one with long angled flexible interconnects, and one with short-angled flexible interconnects. The different variations were included in order to test if either the straight or the angled flexible interconnects would etch out better and to test if there is one configuration that folds down the best. Three of the etched out structures are shown in Fig. 45. All of the different configurations etch out quite well. The circuit area remains well protected even with a significant over-etch, as can be seen by the thick silicon area on the backside of the probe as indicated in Fig. 45. The even width of undercut around the circuit area shows that the front side is now also well protected by the multiple dielectric bridges, even though the flexible interconnects are quite far apart. All the rest of the structure has been cleared to the boron etch stop as it should be; this was true for all four configurations.

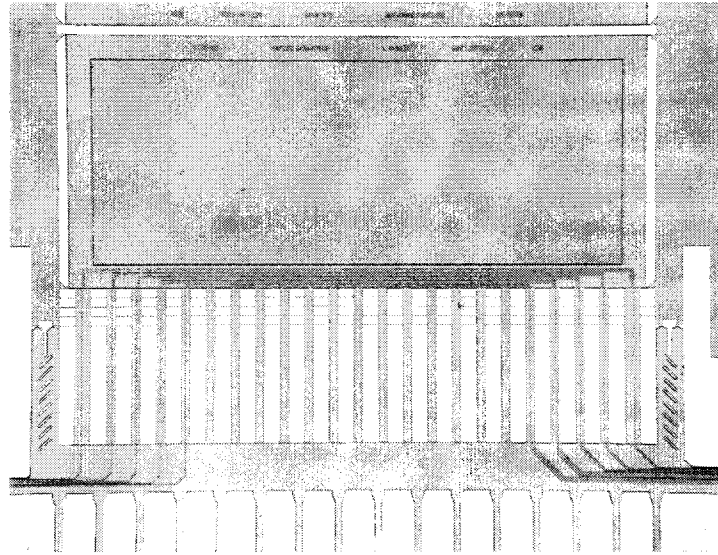


Fig. 44: A photograph of one of the structures for testing the fold-down design of STIM-3B using flexible ribbon cable interconnects as well as the technique for protecting the circuitry from undercut using dielectric bridges.

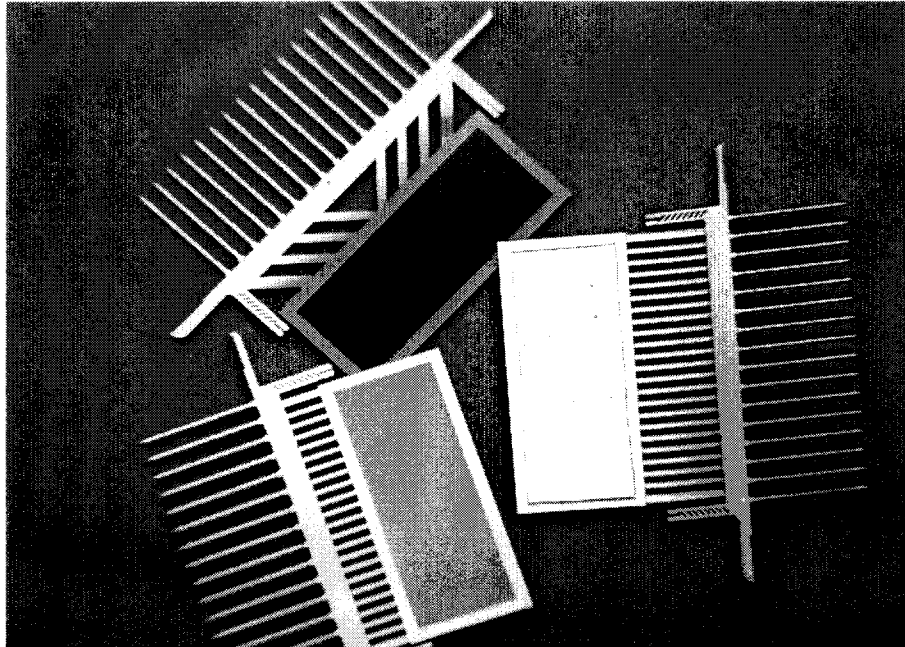


Fig. 45: A photograph of etched-out STIM-3 test structures. Three configurations are shown with the one on the right having its backside turned up, showing the well protected thick silicon circuit area.

6. An External Interface for Active Stimulating Microelectrode Arrays

The active stimulating probes require a support system to provide the necessary power connections and to implement the signaling protocols that effect user-controlled stimulation. We have designed and implemented the components of such a system in the form of a hardware driver unit and accompanying user-interface software. This section describes the two components of this system.

The Hardware Driver Unit

The purpose of the hardware driver unit is to provide power to the stimulating array, to encode stimulus waveforms over two (or three) data lines using a predefined protocol, and to generate pulsatile current waveforms for the stimulating arrays (STIM-2B/-3B) that require off-device current generation. Our main design goals included the following features:

- A maximum serial bit rate of 10 Mbps, thereby enabling stimulus commands to be sent every $2\mu\text{s}$ to a single device (assuming 20 bits of data per command word), or a linear scaling of this quantity for a multi-device configuration.
- A high degree of flexibility in the implementation of the microelectrode array communication protocol in order to support a wide variety of existing and future devices
- A connection to a host computer supporting a broad variety of choices in hardware and operating systems.

Figure 46 diagrams the major components of the hardware driver design. The system is centered on a TMS320C26 digital signal processor (DSP). The choice of a DSP as the central processor reflected the need to write data to the probe circuitry to keep up with a 10 Mbps stimulation rate. DSP processors, in addition to the implementation of common signal processing functions, are also capable of moving data to external devices at high speed. Since the demands on the central processor are otherwise quite moderate, this DSP processor provided an inexpensive answer to the high data rate requirement.

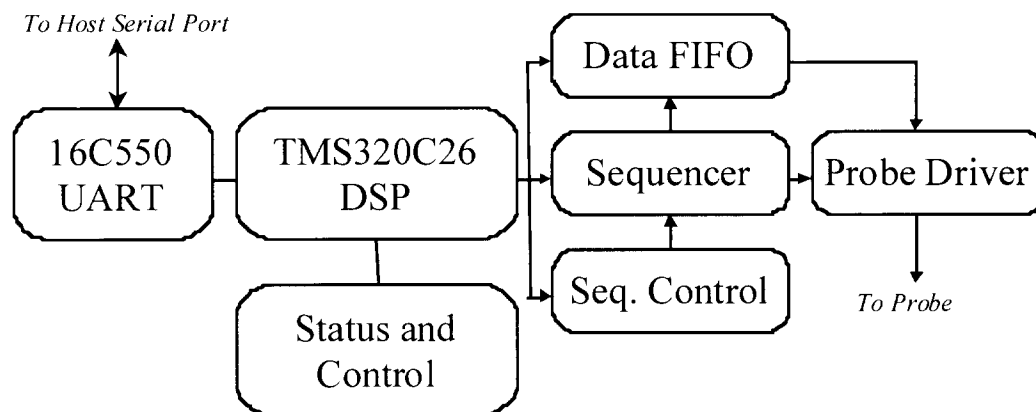


Fig. 46: A block diagram of the hardware driver unit.

The actual microelectrode array data waveforms are generated by a separate processor-like subsystem known as the sequencer. This sequencer is driven by a large data table, software-modifiable in real time, thereby providing the flexibility to support a wide range of array devices. The sequencer co-ordinates both predetermined sections of the communication protocol as well as the stimulus data parameters. This frees the CPU from all aspects of the communication protocol, except for providing the sequencer with the actual stimulus data. A FIFO buffer allows the CPU to write stimulus data to the sequencer without concern for hard and frequent real-time constraints.

The sequencer is clocked from an oscillator that is separate from the CPU and uses a software-programmable divider circuit to allow up to 256 different stimulation bit rates, at sub-multiples of the nominal 10 Mbps rate.

The sequencer generates standard bi-level digital waveforms that encode the necessary stimulus parameters. The probe driver subsystem converts these waveforms to the tri-level voltage waveforms expected by the microelectrode arrays. A set of high-speed low-resistance analog switches are used to convert two bits of digital data to the three logic voltages (+5V, -5V, and 0V) plus a fourth high-impedance state, allowing each probe connection to be effectively isolated from the probe driver.

The final subsystem uses a 16C550C UART as an interface to the industry-standard RS-232 protocol for communication with a remote host computer. This UART contains built-in support for hardware handshaking and buffering, thus freeing the CPU from all tasks other than reading and writing data. This combination allows for reliable constant throughput from the host computer to the hardware driver unit that is nearly independent of processor loading on both the host and remote ends.

The use of an RS-232 communication interface between a host computer and the hardware driver provides the desired independence from a particular choice of computer hardware or operating system. This interface is supported (in both hardware and software) by "Wintel", Apple and Unix platforms. The current implementation of our interface software (described below) has been developed for the IBM PC and Windows 95 platform but the hardware driver unit is in no way dependent upon this combination. The hardware driver unit is currently implemented on a wirewrap carrier, chosen for its ease of testing and modification. An instantiation of this design on a more robust printed circuit board is currently in progress.

The User Interface Software

The human user of the microelectrode stimulating array should not be concerned with the low-level details of the probe communication protocol. Clearly, a high-level user interface is needed to insulate the human user from these details. We have written a graphical user interface (GUI) running under the Windows 95 operating system on a PC computer for just this purpose. This interface uses the RS-232 serial communications support built-in to Windows 95 to communicate with the hardware driver unit.

The main screen of the GUI is shown in Fig. 47. This panel allows the user to specify the amplitude and duration of both phases of a biphasic pulse waveform. The overall repetition rate is also a variable parameter. With these parameters, the user can send one or more consecutive single pulses, as well as initiate continuous stimulation, on any desired channel. A given set of pulse parameters can be saved to disk for future recall. The stimulate/record mode of each channel is also programmable.

Figure 48 shows another panel that a user will normally not use (it initially appears minimized) but is available for lower-level testing or debugging work. This panel allows greater control over the internal working of the hardware driver unit. Among other things, this panel allows initiating a power-on reset of the stimulating array and performing a low-level reset of the sequencer circuitry.

At an even lower lever, Fig. 49 shows a third panel that is to be used even less frequently. This panel shows a command-line interface, based on the Python interpreted programming language, which provides direct control over all aspects of the hardware driver unit. The purpose of this interface is to provide an immediate method of implementing any function on the hardware driver unit, when that function is not supported by the graphical interface. The graphical interface is intended to evolve in response to the requirements of users so that the textual interface should rarely be necessary. The latter exists, however, to put maximum power in the hands of users who need it.

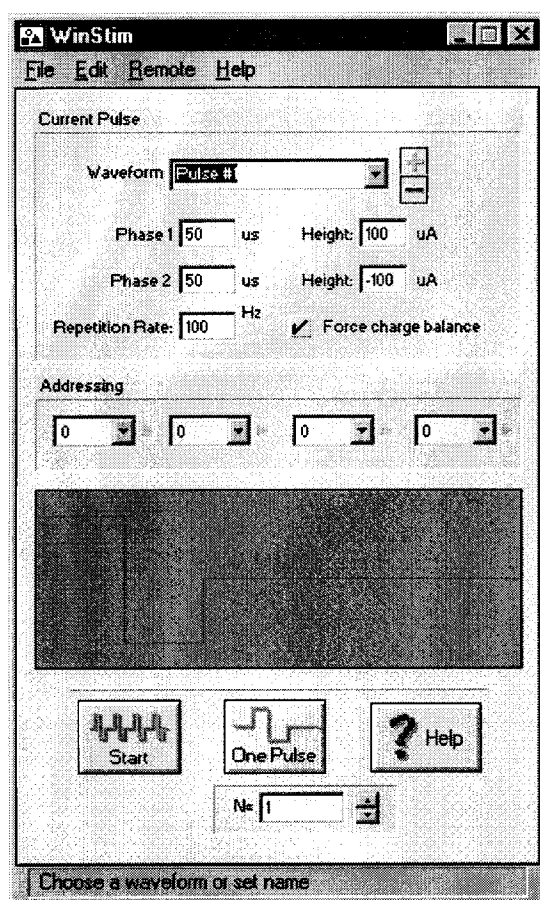


Fig. 47: The main panel of the graphical user interface.

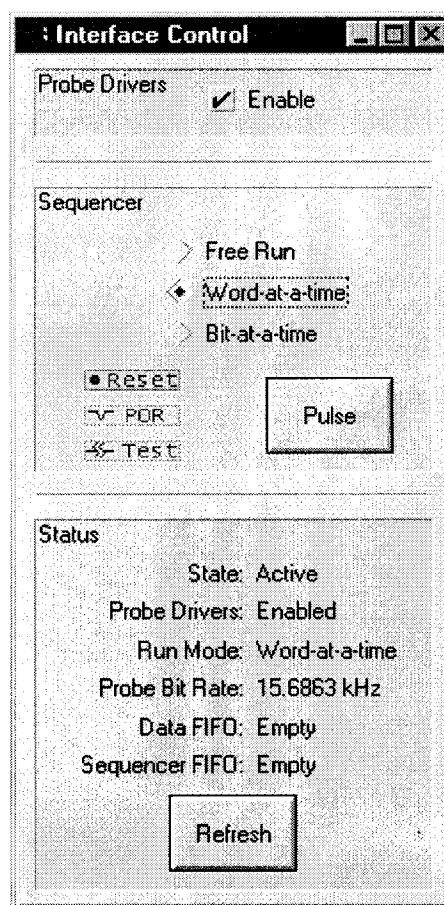
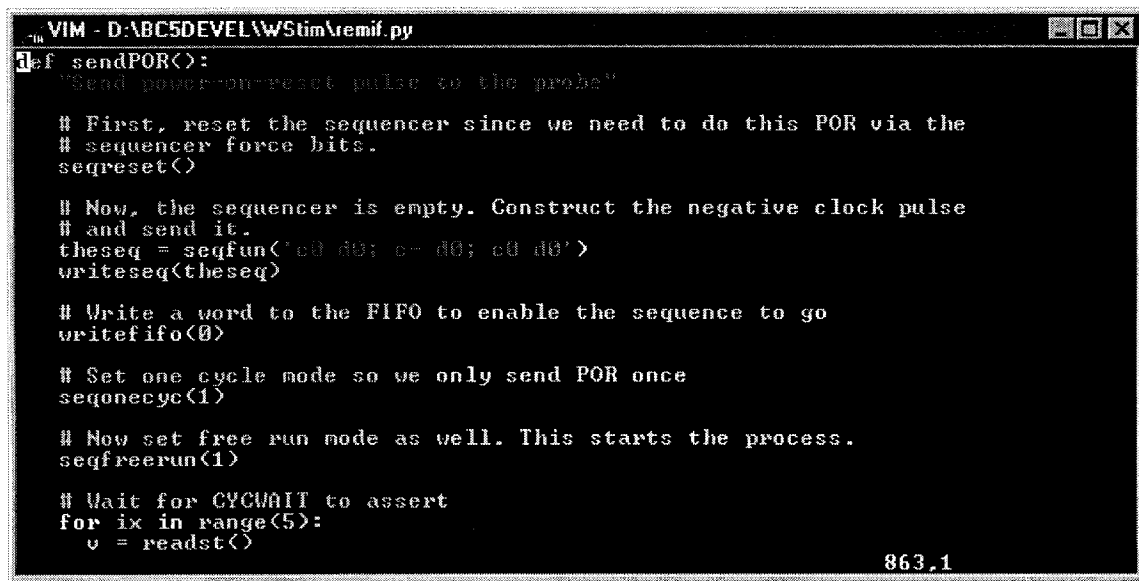


Fig. 48: The interface to lower-level sequencer and probe driver functions.



```
VIM - D:\ABC5DEVEL\W5tim\remif.py
def sendPOR():
    "Send power-on-reset pulse to the probe"

    # First, reset the sequencer since we need to do this POR via the
    # sequencer force bits.
    seqreset()

    # Now, the sequencer is empty. Construct the negative clock pulse
    # and send it.
    theseq = seqfun('c0 d0; c- d0; c0 d0')
    writeseq(theseq)

    # Write a word to the FIFO to enable the sequence to go
    writefifo(0)

    # Set one cycle mode so we only send POR once
    seqonecyc(1)

    # Now set free run mode as well. This starts the process.
    seqfreerun(1)

    # Wait for CYCWAIT to assert
    for ix in range(5):
        v = readst()
```

863.1

Fig. 49: The command-line interface window

7. *Conclusions*

This contract has advanced the state-of-the-art in micromachined stimulating electrode arrays in a number of areas. Improvements in the design of the stimulating sites have eliminated the iridium adhesion problems seen in the past and ensured good step coverage of the site metal into the contact vias. Titanium nitride is being explored as a possible to activated iridium (IrO) as a site material with promising results, and both titanium silicide and tantalum have been shown capable of reducing the resistance of polysilicon interconnect lines by as much as an order of magnitude. A variety of passive probe designs have been fabricated for internal and external users, including a flexible 22-site stimulating probe which could serve as a prototype for an improved cochlear prosthesis. These devices have been conformally coated with parylene for mechanical strength; the sites are exposed using laser ablation followed by an oxygen plasma to remove residual polymer. The use of alternative etch-stop techniques for defining the probe substrate have also been explored, and the use of a bulk n+ buried sacrificial layer has been found capable of forming lightly-doped probe substrates in a single-sided process. This process would allow the formation of distributed circuitry on probe shanks; however, the overall process is somewhat more complex than the boron etch-stop now used. The boron process will be retained for penetrating probes, although for applications such as the cochlear probe the n+ buried layer process has advantages and should be explored further.

The process technology for active probes has been improved to the point where it now allows high yield on a repeatable basis. Improved circuit contacts are ensured using thick titanium plugs under the aluminum circuit metal, and hillocking is avoided in the pad areas using layered titanium-aluminum stacks. Attack of the circuit area during the final probe release etch is prevented using dielectric bridges at the convex corners of the circuit area, and early release of the probe shanks is aided using deep dry etching to allow shank undercutting from the front of the wafer.

A 64-site 4-channel stimulating probe (STIM-2B) with off-chip current generation has been developed under this contract. The probe accepts a serial bit stream to select four of the 64 sites using four 16:1 multiplexers. Any site can be set to either stimulation or recording, with on-chip band-limited preamplifiers provided for each channel. The probe allows impedance testing from off-chip as well as parallel activation of the various sites. The probes have been characterized in-vitro and found to provide performance very close to design targets. They are now being used in-vivo to map connections between the dorsal cochlear nucleus and the inferior colliculus in guinea pig. Mapping that would be impossible using individual wire electrodes can be performed automatically without physically moving the probes via electronic site positioning/selection. Versions of this probe that are compatible with use in three-dimensional arrays (STIM-3B) have also been realized along with the required platforms and spacers. Microassemblies as large as 1024 sites and 64 parallel channels can be realized and are being assembled.

The previously-designed high-end probe STIM-2 was fabricated and tested in-vitro under this contract. Most aspects of these probes performed close to expectations; however, some areas for design improvement were identified, including the need for redesigned digital-to-analog converters for stimulus current generation. We are now implementing the needed design changes prior to a final fabrication run. A modular DSP-based external user interface for both STIM-2B/3B and STIM-2/3 has been developed and is now in use with these probes. The interface includes a graphical user interface to make the probes simple to use.

In the future, we plan on extensive testing of STIM-2B in-vivo to demonstrate the utility of these probes in neurophysiological studies. We also plan to develop STIM-3B as a vehicle for prosthesis experiments in the auditory and visual systems. STIM-2 and STIM-3 will be developed as high-end implementations of the technology, and we will develop implantable telemetry systems capable of replacing the present percutaneous plug with a wireless interface, serving at least one implanted probe. This technology, developed as the result of support from the Neural Prosthesis Program, is becoming widely used in the neuroscience community and should soon make possible key experiments to establish the performance possible in several important neural prostheses.

8. References

- [Anderson 89] D. J. Anderson, K. Najafi, S. J. Tanghe, D. A. Evans, K. L. Levy, J. F. Hetke, X. Xue, J. J. Zappia, K. D. Wise. Batch-Fabricated Thin-Film Electrodes for Stimulation of the Central Auditory System. *IEEE Trans. Biomed. Eng.* 36:693-704, 1989.
- [Bagshaw 76] E.V. Bagshaw and M.H Evans (1976) Measurement of current spread from microelectrodes when stimulating within the nervous system. *Exp. Brain Res.* 25: 391-400.
- [Bai 98] Q. Bai, M. Gingerich, and K. D. Wise, "An Active Three-Dimensional Microelectrode Array for Intracortical Recording," *Digest Solid-State Sensor and Actuator Workshop*, Hilton Head, pp. 15-18, June 1998.
- [Beebe 88] X. Beebe, T. L. Rose. Charge injection limits of activated iridium oxide electrodes with 0.2 ms pulses in bicarbonate buffered saline. *IEEE Trans. Biomed. Eng.* 35:494-495, 1988.
- [Chen 97] J. Chen, K. D. Wise, J. F. Hetke, and S. C. Bledsoe, Jr., "A Multichannel Neural Probe for Selective Chemical Delivery at the Cellular Level," *IEEE Trans. Biomed. Engr.*, 44, pp. 760-769, August 1997.
- [Drake 88] K. L. Drake, K. D. Wise, J. Farraye, D. J. Anderson, and S. L. BeMent. Performance of planar multisite microprobes in recording extracellular single-unit intracortical activity. *IEEE Trans. Biomed. Eng.*, 35:719-732, 1988.
- [Hetke 94] J. F. Hetke, J. L. Lund, K. Najafi, K. D. Wise, and D. J. Anderson, "Silicon Ribbon Cables for Chronically Implantable Microelectrodes Arrays," *IEEE Trans. Biomed. Eng.*, vol. 41, pp. 314-321, April 1994.
- [Janders 96] M. Janders, U. Egert, M. Stelzle, W. Nisch, "Novel Thin-Film Titanium Nitride Microelectrodes with Excellent Charge Transfer Capability for Cell Stimulation and Sensing Applications," *Digest EMBS*, Amsterdam, October 1996.
- [Ji 90] J. Ji and K. D. Wise, "An Implantable CMOS Analog Signal Processor for Multiplexed Microelectrode Recording Arrays," *Digest 1990 IEEE Solid-State Sensor and Actuator Workshop*, Hilton Head, S.C., pp. 107-110, June 1990.

- [Ji 92] J. Ji, K. D. Wise. An Implantable CMOS Circuit Interface for Multiplexed Microelectrode Recording Arrays. *IEEE J. of Solid-State Circuits*, Vol. SC-26, no. 3, pp. 433-443, Mar. 1992.
- [Ji 92-2] J. Ji, S.T. Cho, Y. Zhang, K. Najafi, and K.D. Wise, "An Ultraminiature CMOS Pressure Sensor For a Multiplexed Cardiovascular Catheter," *IEEE Trans. Electron Devices*, Vol. 39, No. 10, pp. 2260-2267, October 1992
- [Kim 93] C. Kim, S. J. Tanghe, and K. D. Wise, "Multichannel Neural Probes with On-Chip CMOS Circuitry and High-Current Stimulating Sites," *Digest IEEE Int. Conf. on Solid-State Sensors and Actuators (Transducers'93)*, Yokohama, pp. 454-457, June 1993.
- [Kim 94-1] C. Kim and K. D. Wise, "A 64-Site Multiplexed Low-Profile Neural Probe with On-Chip CMOS Circuitry," *Digest 1994 IEEE Symposium on VLSI Circuits*, Honolulu, pp. June 1994.
- [Kim 94-2] Changhyum Kim, A 64-Site Multiplexed Low-Profile Neural Probe for use in Neural Prostheses, Ph.D. Dissertation, The University of Michigan, 1994.
- [Kim 96] C. Kim and K. D. Wise, "A 64-Site Multishank CMOS Low-Profile Neural Stimulating Probe," *IEEE J. Solid-State Circuits*, 31, pp. 1230-1238, September 1996.
- [Lund 94] J. L. Lund and K. D. Wise, "Chip-Level Encapsulation of Implantable CMOS Microelectrode Arrays," *Digest Solid-State Sensor and Actuator Workshop*, Hilton Head, S.C., pp. 29-32, June 1994.
- [Najafi 85] K. Najafi, K. D. Wise, and T. Mochizuki, "A high-yield IC-compatible multichannel recording array," *IEEE Trans. Electron Devices*, 32:1206-1211, 1985.
- [Najafi 90-1] K. Najafi, J. Ji, and K. D. Wise, "Scaling Limitations of Silicon Multichannel Recording Probes," *IEEE Trans. Biomed. Eng.*, 37:1-10, 1990.
- [Najafi 90-2] K. Najafi, and J.F. Hetke, "Strength Characterization of Silicon Microprobes in Neurophysiological Applications," *IEEE Trans. on Biomed. Eng.*, Vol. 37, No. 5, pp. 474-481, May 1990.
- [Nardin 95] M. Nardin, and K. Najafi, "A Multichannel Neuromuscular Microstimulator With Bi-Directional Telemetry," *1995 Int. Conference on Solid-State Sensors and Actuators, Transducers '95*, pp. 59-62, Stockholm, Sweden, June 1995
- [Robblee 90-1] L. S. Robblee, S. F. Cogan, T. L. Rose, D. V. Hills, A. G. Kimball. Studies of the electrochemistry of stimulating electrodes. Eighth quarterly progress report for the National Institute of Health, Contract no. NO1-NS-8-2313, November, 1990
- [Robblee 90-2] L. S. Robblee, T. L. Rose. *Neural Prostheses: Fundamental Studies*, W. Agnew, D. McCreery, Ed., chapter 2, Englewood Cliffs, New Jersey, 1990.
- [Rousche 92] P. J. Rousche and R. A. Normann, "A Method for Pneumatically Inserting an Array of Penetrating Electrodes into Cortical Tissue," *Annals of Biomedical Engineering*, 20, pp. 413-422, 1992.

- [Seidel 90] H. Seidel, L. Csepregi, A. Heuberger, and H. Baumgartel, "Anisotropic Etching of Crystalline Silicon in Alkaline Solutions," *J. Electrochem. Soc.*, pp. 3612-3632, November 1990.
- [Tanghe 92-1] S. J. Tanghe and K. D. Wise, "A 16-Channel CMOS Neural Stimulating Array," *IEEE J. Solid-State Circuits*, vol. 27, pp. 1819-1825, Dec. 1992.
- [Tanghe 92-2] Steven J. Tanghe, Micromachined Silicon Stimulating Probes with CMOS Circuitry for use in the Central Nervous System, Ph.D. Dissertation, The University of Michigan, 1992.
- [Wise 91-1] K. D. Wise and K. Najafi, "Microfabrication Techniques for Integrated Sensors and Microsystems," (Invited), *Science*, November 29, 1991.
- [Wise 91-2] K. D. Wise and N. Najafi, "The Coming Opportunities in Microsensor Systems," (Invited), *Digest IEEE Int. Conf. on Solid-State Sensors and Actuators*, San Francisco, pp. 2-7, June 1991.
- [Wise 96] K. D. Wise, "Microelectromechanical Systems: Interfacing Electronics to a Non-Electronic World," (Invited Plenary), Technical Digest, *International Electron Devices Meeting*, San Francisco, pp. 11-18, December 1996.